ISSN 1063-7796, Physics of Particles and Nuclei, 2020, Vol. 51, No. 5, pp. 829–858. © Pleiades Publishing, Ltd., 2020.

Search for Dark Sector Physics with NA64

S. N. Gninenko[a], N. V. Krasnikov[a, b, *], and V. A. Matveev[a, b]

[a] *INR RAS, Moscow, 117312 Russia*

[b] *Joint Institute for Nuclear Research, Dubna, 141980 Russia*

**e-mail: Nikolai.Krasnikov@cern.ch*

Received January 12, 2020; revised February 12, 2020; accepted March 13, 2020

Abstract—The NA64 experiment consists of two detectors which are planned to be located at the electron (NA64e) and muon (NA64μ) beams of the CERN SPS and start operation after the LHC long-stop 2 in 2021. Its main goals include searches for dark sector physics—particularly light dark matter (LDM), visible and invisible decays of dark photons (A'), and new light particles that could explain the ^{8}Be and $g_\mu - 2$ anomalies. Here we review these physics goals, the current status of NA64 including recent results and perspectives of further searches, as well as other ongoing or planned experiments in this field. The main theoretical results on LDM, the problem of the origin of the γ-A' mixing term and its connection to loop corrections, possible existence of a new light Z' coupled to $L_\mu - L_\tau$ current are also discussed.

DOI: 10.1134/S1063779620050044

1. INTRODUCTION

At present the most striking evidence in favour of new physics beyond the Standard model (SM) is the observation of Dark Matter (DM) [1, 2]. The nature of DM is one of challenging questions in physics. If DM is a thermal relic from the hot early Universe then its existence motivates to look for models with nongravitational interactions between dark and ordinary matter. There is a lot of candidates for the role of dark matter [1, 2]. In particular, there are LDM(light dark matter) models [3–7] with the mass of DM particles $\leq 0(1)$ GeV. LDM particles with masses below 0(1) GeV were generally expected to be ruled out because they overclose the Universe [8]. However there are models [3–7] with additional light vector boson and LDM particles that avoid the arguments [8] excluding the LDM. The standard assumption that in the hot early Universe the DM particles are in equilibrium with ordinary matter is often used. During the Universe expansion the temperature decreases and at some point the thermal decoupling of the DM starts to work. Namely, at some freeze-out temperature the annihilation cross-section of DM paricles

$$\text{DM particles} \to \text{SM particles}$$

becomes too small to obey the equilibrium of DM particles with the SM particles and the DM decouples. The experimental data are in favour of scenario with cold relic for which the freeze-out temperature is much lower than the mass of the DM particle. In other words the DM particles decouple in non-relativistic regime. The value of the DM annihilation cross-section at the decoupling epoch determines the value of the current DM density in the Universe. Too big annihilation cross-section leads to small DM density and vise versa too small annihilation cross section leads to DM overproduction. The observed value of the DM density fraction $\frac{\rho_d}{\rho_c} \approx 0.23$ [9] allows to estimate the DM annihilation cross-section into the SM particles and hence to estimate the discovery potential of the LDM both in direct underground and accelerator experiments. Namely, the annihilation cross-section leading to the correct DM density is estimated to be $\sigma_{an} \sim 1$ pbn and the value of the cross-section depends rather weakly on the DM mass [1, 2]. Models with the LDM ($m_\chi \leq 1$ GeV) can be classified by the spins and masses of the DM particles and mediator. The scalar DM mediator models are severely restricted [10, 11] but not completely excluded by rare K- and B-meson decays. Models with light vector bosons [4, 12, 13] (vector portal) are rather popular now. In these models light vector boson A' mediates between our world and the dark sector [4]. Another possible hint in favour of new physics is the muon $g_\mu - 2$ anomaly which is the 3.6σ discrepancy between the experimental values [14, 9] and the SM predictions [15–18] for the anomalous magnetic moment of the muon. Among several extensions of the SM explaining the $g_\mu - 2$ anomaly, the models predicting the existence of a weak leptonic force mediated by a sub-GeV gauge boson Z' that couples predominantly to the difference between the muon and tau lepton currents,

$L_\mu - L_\tau$, are of general interest. The abelian symmetry $L_\mu - L_\tau$ is an anomaly-free global symmetry within the SM [19–21]. The $L_\mu - L_\tau$ gauge symmetry breaking is crucial for the appearance of a new relatively light, with a mass $m_{Z'} \le 1$ GeV, vector boson (Z') which couples very weakly to muon and tau-lepton with the coupling constant $\alpha_\mu \sim O(10^{-8})$ [22–25] and explain muon $g_\mu - 2$ anomaly. Recent claim [26] of the discovery of 17 MeV vector particle observed as a peak in e^+e^- invariant mass distribution in nuclear transitions makes the question of possible light vector boson existence extremely interesting and important and enhance motivation for the experimental searches at low energy intensity frontier.

At present the most popular vector mediator model is the model with additional light vector boson A' (dark photon) [4, 13] which couples to the SM electromagnetic current. However other light vector boson models, in particular, model with $L_\mu - L_\tau$ interaction [27–30], are possible as messenger candidates beetween our world and DM world.

The aim of this paper is review of the search for LDM at the NA64 fixed target experiment [31–35] at CERN and related current and future experiments on the search for LDM. Also we review essential part of the phenomenology related with the LDM models. The paper is organized as follows. In section 2 we describe phenomenology of the dark photon model. In particular, we discuss the bound on low energy effective coupling constant $\bar{\alpha}_d(m_{A'}) \equiv \alpha_d$ derived from the requirement of the absence of Landau pole singularity up to some scale $\Lambda_{\rm pole}$. We present the main formulae for the A' electroproduction reaction $eZ \to eZA'$ on nuclei. We review muon $g_\mu - 2$ anomaly and the possibility to explain it due to existence of new light vector boson interacting with muons. Also we discuss the problem of the origin of photon-dark photon mixing term $\frac{\epsilon}{2}F^{\mu\nu}F'_{\mu\nu}$ and its connection with loop corrections. In sections 3 we review current accelerator and nonaccelerator bounds including experiments on direct LDM detection. In section 4 we describe the NA64 experiment on the search for both invisible and visible A' boson decay. In section 5 we review the last NA64 results and discuss future NA64 perspectives on the search for LDM and, in particular, we discuss the NA64 LDM discovery potential with the use of muon beam. In section 6 we outline some other future experiments related with the search for dark photon and LDM at NA64. Section 7 contains the main conclusions. In Appendix A we collect the main formulae used for the approximate DM density calculations. In Appendix B we discuss the discovery potential of NA64 for the case of visible dark photon A' decays $A' \to \chi_1\chi_2 \to e^+e^-\chi_1\chi_1$ with large missing energy.

2. A LITTLE BIT OF THEORY

2.1. Model with Dark Photon

In model with "dark photon" [4, 13] new light vector boson (dark photon) A' interacts with the Standard $SU_c(3) \otimes SU_L(2) \otimes U(1)$ gauge model only due to kinetic mixing with $U'(1)$ gauge field A'_μ. Dark photon interacts also with LDM. In renormalizable models DM particles have spin 0 or 1/2. The Lagrangian of the model has the form

$$L = L_{\rm SM} + L_{\rm SM,dark} + L_{\rm dark}, \tag{1}$$

where $L_{\rm SM}$ is the SM Lagrangian,

$$L_{\rm SM,dark} = -\frac{\epsilon}{2\cos\theta_w} B^{\mu\nu}F'_{\mu\nu}, \tag{2}$$

$B^{\mu\nu} = \partial^\mu B^\nu - \partial^\nu B^\nu$, $F'_{\mu\nu} = \partial_\mu A'_\nu - \partial_\nu A'_\mu$ and the $L_{\rm dark}$ is the DM Lagrangian[1]. For Dirac LDM χ the DM Lagrangian is

$$\begin{aligned} L_{\rm dark} &= -\frac{1}{4}F'_{\mu\nu}F'^{\mu\nu} + i\bar{\chi}\gamma^\mu\partial_\mu\chi - m_\chi\bar{\chi}\chi \\ &+ e_d\bar{\chi}\gamma^\mu\chi A'_\mu + \frac{m^2_{A'}}{2}A'_\mu A'^\mu, \end{aligned} \tag{3}$$

The abelian gauge symmetry

$$A'_\mu \to A'_\mu + \partial_\mu\alpha, \tag{4}$$

$$\chi \to \exp(ie_d\alpha)\chi \tag{5}$$

is explicitly broken due to the mass term $\frac{m^2_{A'}}{2}A'_\mu A'^\mu$ in the Lagrangian (3). However we can use the Higgs mechanism for dark photon A'_μ mass creation, namely we can use the Lagrangian

$$L_\phi = (\partial_\mu\phi - ie_dA'_\mu\phi)(\partial^\mu\phi - ie_dA'^\mu\phi)^* - \lambda(\phi^*\phi - c^2)^2. \tag{6}$$

Here ϕ is scalar field. The spontaneous breaking of the gauge symmetry (4), (5) due to $\langle\phi\rangle \ne 0$ leads to nonzero dark photon mass. As a consequence of the mixing term $L_{\rm SM,dark} = -\frac{\epsilon}{2\cos\theta_w}B^{\mu\nu}F'_{\mu\nu}$ the low energy interaction between dark photon A'_μ and the SM fermions is described by the effective Lagrangian

$$L_{A',\rm SM} = \epsilon eA'_\mu J^\mu_{em}, \tag{7}$$

[1] Here B_μ is the SM $U(1)$ gauge field.

where J^{μ}_{em} is the SM electromagnetic current. The invisible and visible decay rates of A' for fermion DM particles χ are given by

$$\Gamma(A' \to \chi\bar{\chi}) = \frac{\alpha_D}{3} m_{A'} \left(1 + \frac{2m_\chi^2}{m_{A'}^2}\right)\sqrt{1 - \frac{4m_\chi^2}{m_{A'}^2}}, \quad (8)$$

$$\Gamma(A' \to e^+e^-) = \frac{\epsilon^2\alpha}{3} m_{A'} \left(1 + \frac{2m_e^2}{m_{A'}^2}\right)\sqrt{1 - \frac{4m_e^2}{m_{A'}^2}}. \quad (9)$$

Here $\alpha = \frac{e^2}{4\pi} = 1/137$ and $\alpha_a = \frac{e_d^2}{4\pi}$ is the analog of the electromagnetic fine coupling constant for dark photon. For scalar DM particles χ the invisible decay width is

$$\Gamma(A' \to \chi\chi^*) = \frac{\alpha_D}{12} m_{A'} \left(1 - 4\frac{m_\chi^2}{m_{A'}^2}\right)\sqrt{1 - \frac{4m_\chi^2}{m_{A'}^2}}. \quad (10)$$

2.2. Upper Bound and Range of α_D

One can obtain upper bound on α_D by the requirement of the absence of Landau pole singularity for the effective coupling constant p up to some scale $n = 0$ [36]. One loop β-function for $\bar{\alpha}_D(\mu)$ is

$$\beta(\bar{\alpha}_D) = \frac{\bar{\alpha}_D^2}{2\pi}\left[\frac{4}{3}\left(Q_F^2 n_F + Q_S^2\frac{n_S}{4}\right)\right]. \quad (11)$$

Here $\beta(\bar{\alpha}_D) \equiv \mu\frac{d\bar{\alpha}_D}{d\mu}$ and n_F (n_s) is the number of fermions (scalars) with the $U'(1)$ charge $Q_F(Q_S)$. For the model with pseudo-Dirac fermion [37] we have to introduce an additional scalar with $Q_S = 2$ to realize nonzero splitting between fermion masses, so one loop β-function is $\beta(\bar{\alpha}_D) = \frac{4\bar{\alpha}_D^2}{3\pi}$. For the model with Majorana fermion we also have to introduce an additional scalar field with the charge $Q_S = 2$ and additional Majorana field to cancel γ_5-anomalies, so the β-function coincides with the β-function for the model with pseudo-Dirac fermions. For the model with charged scalar DM to create nonzero dark photon mass in a gauge invariant way we have to introduce additional scalar field with $Q_S = 1$, so one loop β-function is $\beta = \alpha^2/3\pi$. From the requirement that $\Lambda \geq 1$ TeV [36] we find that $\alpha_D \leq 0.2$ for pseudo-Dirac and Majorana fermions and $\alpha_D \leq 0.8$ for charged scalars [2]. Here α_D is an effective low energy coupling constant at scale $\mu \sim m_{A'}$, i.e. $\alpha_D = \bar{\alpha}_D(m_{A'})$. In our calculations as a reper point we used the value $m_{A'} = 10$ MeV. In the assumption that dark photon model is valid up to Planck scale, i.e. $\Lambda = M_{PL} = 1.2\times10^{19}$ GeV, we find that for pseudo-Dirac and Majorana fermions $\alpha_D \leq 0.05$ while for scalars $\alpha_D \leq 0.2$. In the SM the $SU_c(3)$, $SU_L(2)$ and $U(1)$ gauge coupling constants are equal to $\sim(1/30 - 1/50)$ at the Planck scale. It is natural to assume that the effective gauge coupling $\bar{\alpha}_D(\mu = M_{PL})$ is of the order of $SU_c(3)$, $SU_L(2)$ and $U(1)$ gauge coupling constants, i.e. $\bar{\alpha}_D(\mu = M_{PL}) \sim (1/30 - 1/50)$. As a result of this assumption we find that the values of the low energy coupling α_D in the range $\alpha_D \sim (0.015–0.02)$ are the most natural.

2.3. Some Comments on the Origin of the Mixing Parameter ϵ

In Holdom paper [13][3] the origin of the mixing ϵ parameter was assumed to be related with radiative corrections. To clarify this statement consider the simplest model with two free $U(1) \otimes U'(1)$ gauge fields A_μ and A'_μ. The Lagrangian of the model is

$$L_o = -\frac{1}{4}F_{\mu\nu}F^{\mu\nu} - \frac{1}{4}F'_{\mu\nu}F'^{\mu} + \frac{m_{0,A'}^2}{2}A'^{\mu}A'_{\mu} - \frac{1}{2}\epsilon_{0l}F'_{\mu\nu}F^{\mu\nu}, \quad (12)$$

where $F_{\mu\nu} = \partial_\mu A_\nu - \partial_\nu A_\mu$ and $F'_{\mu\nu} = \partial_\mu A'_\nu - \partial_\nu A'_\mu$. For $\epsilon_{0l} = 0$ the Lagrangian (12) is invariant under two independent discrete symmetries $A_\mu \to -A_\mu$ and $A'_\mu \to -A'_\mu$. After diagonalization we find that the spectrum of the model for $|\epsilon_{0l}| \ll 1$ consists of massless vector particle(photon) and massive vector particle(dark photon) with a mass $m_{A'}^2 = m_{0,A'}^2(1 + \epsilon_{0l}^2)$. Let us add to the model massive fermion field ψ_M with a mass M which interacts both with A_μ and A'_μ with the interaction Lagrangian

$$\Delta L = e\bar{\psi}\gamma^\mu\psi A_\mu + e'\bar{\psi}\gamma^\mu\psi A'_\mu. \quad (13)$$

At one-loop level the propagator $\int e^{ipx}\langle T(A_\mu(x)A_\nu(0))\rangle d^4x$ depends on virtual momentum p^2. It means that one-loop correction ϵ_{1l} depends on virtual momentum p^2, namely

$$\epsilon_{1l}(p^2) = \frac{ee'}{16\pi^2}\int_{-1}^{1}(1-\eta^2)\ln\left[\frac{4M^2 - p^2(1-\eta^2)}{\mu^2}\right]d\eta. \quad (14)$$

[2] For smaller values of Λ we shall have charged particles in the specrtrum with masses ≤ 1 TeV [36] that contradicts to the LHC bounds.

[3] Recent discussion of the ϵ parameter origin is contained in ref. [38].

Here μ is some renormalization point, so one-loop contribution to the tree level ϵ_{0l} parameter depends on the renormalization scheme. To our mind the most natural choice of the renormalization point μ is to require that radiative corrections to the tree level ϵ_{0l} parameter vanish at the A' mass shell

$$\epsilon_{1l}(p^2 = m^2_{0,A'}) = 0. \quad (15)$$

The renormalization condition (15) guarantees us that radiative corrections don't modify the tree level formula $m^2_{A'} = m^2_{0,A'}(1+\epsilon^2_{0l})$ for the pole dark photon mass. The renormalization condition (15) leads to well defined value of the ϵ parameter at one-loop level

$$\epsilon_{0+1l}(p^2) = \epsilon_{0l} + \frac{ee'}{16\pi^2} \times \int_{-1}^{1}(1-\eta^2)\ln\left[\frac{4M^2 - p^2(1-\eta^2)}{4M^2 - m^2_{0,A'}(1-\eta^2)}\right]d\eta. \quad (16)$$

For the normalization condition (15) one-loop contribution to the ϵ_{0l} parameter vanishes as $\epsilon_{1l} \sim \frac{1}{M^2}$ for large fermion masses $M \gg m_{0,A'}$, that agrees with the decoupling expectations. For the model with two massive fermions ψ_1, ψ_2 with masses M_1, M_2, the charges e, e' and $e, -e'$ one-loop correction to the ε_{0l} parameter is ultraviolet finite and it does not depend on the renormalization point μ

$$\epsilon^{\text{naive}}_{1l}(p^2) = \frac{ee'}{16\pi^2} \times \int_{-1}^{1}(1-\eta^2)\ln\left[\frac{4M_1^2 - p^2(1-\eta^2)}{4M_2^2 - p^2(1-\eta^2)}\right]d\eta. \quad (17)$$

However the $\epsilon^{\text{naive}}_{1l}(0) = \frac{ee'}{12\pi^2}\ln\left[\frac{M_1^2}{M_2^2}\right]$ does not vanish for $M_1 \to \infty$, $M_2 \to \infty$ in contradiction with naive decoupling expectations. To cure this situation we can add one-loop finite counter-term $-\frac{\Delta_{1l}}{2}F'_{\mu\nu}F^{\mu\nu}$ to the Lagrangian (12) with $\Delta_{1l} = -\epsilon_{1l}(p^2 = m^2_{A'})$, so one-loop expression for $\epsilon_{1l}(p^2)$ reads

$$\epsilon_{1l}(p^2) = \epsilon^{\text{naive}}_{1l}(p^2) - \epsilon^{\text{naive}}(p^2 = m^2_{0,A'}). \quad (18)$$

One can find that $\epsilon_{1l}(0) \to 0$ for $M_1 \to \infty$, $M_2 \to \infty$ in accordance with decoupling expectations. Let us formulate our main conclusion—within the abelian $U(1)\otimes U'(1)$ gauge model we can't predict the value of the mixing parameter ϵ and to our mind the most natural renormalization scheme is based on the use of the condition that loop corrections to the $\epsilon(p^2)$ vanish at the A' mass shell, so ϵ_{0l} is free arbitrary parameter of the model.

The situation with the ϵ prediction changes drastically if we assume that one of the $U(1)$ abelian gauge groups arises due to gauge symmetry breaking of nonabelian gauge group. As a simplest example consider the model where dark photon originates from $SU'(2)$ gauge symmetry breaking $SU'(2) \to U'(1)$. The unbroken $U(1)\otimes SU'(2)$ gauge symmetry prohibits the mixing term $-\frac{\epsilon}{2}F^{\mu\nu}F'_{\mu\nu}$. Suppose $SU'(2)$ gauge symmetry is broken to $U'(1)$ due to the Higgs field Φ_b ($b = 1, 2, 3$) in adjoint representation. The $U(1)\otimes U'(1)$ mixing term arises as a result of $SU'(2)$ breaking due to the effective term $\frac{\Phi_a}{\Lambda}F'^{a}_{\mu\nu}F^{\mu\nu}$. Suppose we have doublet(under $SU'(2)$) of vector-like fermions ψ_a ($a = 1, 2$) with the mass M and the $U(1)$ charge e. The Yukawa interaction of vector-like fermions with scalar triplet Φ_b is $L_{\text{Yuk}} = -h\Phi_a\bar{\psi}\sigma_a\psi$. Nonzero vacuum expectation value $\langle\Phi_3\rangle \neq 0$ leads to $SU'(2) \to U'(1)$ gauge symmetry breaking and to the splitting of fermion masses for fermion doublet ψ_a, namely $M_{1,2} = M \pm h\langle\Phi_3\rangle$. As a consequence of fermion doublet mass splitting we find nonzero one-loop contribution to the ϵ parameter, namely

$$\varepsilon_{1l} = \frac{eg}{6\pi^2}\ln\left[\frac{M + h\langle\Phi_3\rangle}{M - h\langle\Phi_3\rangle}\right]. \quad (19)$$

Here g is the $SU(2)$ gauge coupling. The expresssion (19) vanishes for $\langle\Phi_3\rangle = 0$ and for $M \to \infty$. For $M \gg h\langle\Phi_3\rangle$ the ε parameter is

$$\epsilon_{1l} = \frac{eg}{6\pi^2}\frac{2h\langle\Phi_3\rangle}{M}. \quad (20)$$

So we find that for the model with nonabelian extension of one of the $U(1)$ gauge groups the ϵ parameter arises as a result of nonabelian gauge symmetry breaking and in principle but not in practise we can predict it as a function of the parameters of the model. To conclude we can say that at present state of art we can't predict reliably the value of the ε parameter.

2.4. Dark Photon Production

There are several A' production mechanisms [4]. In proton nucleus collisions the A' are produced mainly in π^0/η decays $\pi^0/\eta \to \gamma A'$. The use of visible $A' \to e^+e^-$ decay allows to detect dark photon A' as a peak in the e^+e^- invariant mass distribution. Also direct A' production in proton nucleus collisions is possible in full analogy with the photoproduction in proton nucleus collisions.

Other perspective way is the A' production in electron nucleus interactions, namely the use of the reaction

$$e^-(p) + Z(P_i) \to e^-(p') + Z(P_f) + A'(k). \quad (21)$$

Here $p = (E_0, \vec{p})$ is the 4-momentum of incoming electron, $P_i = (M, 0)$ denotes the Z nucleus 4-momentum in the initial state, final state Z nucleus momentum is defined by $P_f = (P_f^0, \vec{P}_f)$, the A'-boson momentum is $k = (k_0, \vec{k})$ and $p' = (e', \vec{p}')$ is the momentum of electron recoil. In the improved Weizsacker–Williams (IWW) approximation the differential and total cross-sections for the reaction (21) for $m_{A'} \gg m_e$ can be written[4] [39] as

$$\frac{d\sigma_{WW}^{A'}}{dx} = (4\alpha^3\epsilon^2\chi_{\rm eff}) \times (1 - x + x^2/3)\left(m_{A'}^2\frac{1-x}{x} + m_e^2 x\right)^{-1}, \quad (22)$$

$$\sigma_{WW}^{A'} = \frac{4}{3}\frac{\epsilon^2\alpha^3}{m_{A'}^2}\chi_{\rm eff}\log(\delta_{A'}^{-1}), \quad (23)$$

$$\delta_{A'} = \max\left[\frac{m_e^2}{m_{A'}^2}, \frac{m_{A'}^2}{E_0^2}\right], \quad (24)$$

where $\chi_{\rm eff}$ is an effective flux of photons

$$\chi_{\rm eff} = \int_{t_{\min}}^{t_{\max}} dt\frac{t - t_{\min}}{t^2}[G_2^{\rm el}(t) + G_2^{\rm inel}(t)], \quad (25)$$

and $x = \dfrac{E_{A'}}{E_o}$. Here $t_{\min} = m_{A'}^4/4E_0^2$, $t_{\max} = m_{A'}^2 + m_e^2$ and $G_2^{\rm el}(t)$, $G_2^{\rm inel}(t)$ are elastic and inelastic form-factors respectively. For NA64 energies $E \le 100$ GeV the elastic form-factor dominates. The elastic form-factor can be represented in the form [39]

$$G_2^{\rm el} = \left(\frac{a^2 t}{1 + a^2 t}\right)^2\left(\frac{1}{1 + t/d}\right)^2 Z^2, \quad (26)$$

where $a = 111Z^{-1/3}/m_e$, $d = 0.164$ GeV$^2A^{-2/3}$ and A is atomic number of nuclei. We consider the quasielastic reaction (21) so the inelastic nuclear formfactor is not taken into account. Numerically, $\chi_{\rm eff} = Z^2\log$, where the function log ~ (5–10) and it depends weakly on atomic screening, nuclear size effects and kinematics.

[4] Exact tree level calculations for the $e^-Z \to e^-ZA'$ reaction have been performed in refs. [40, 41]. For a certain kinematic region of the parameters $m_{A'}, E_A$, the A' yeld derived in the IWW approximation could differ significantly from the exact tree level calculations [40, 41].

2.5. Muon $g_\mu - 2$ Anomaly and the Light Vector Boson Z'

Recent precise measurement of the anomalous magnetic moment of the positive muon $a_\mu = (g_\mu - 2)/2$ from Brookhaven AGS experiment 821 [14] gives result which is about 3.6σ higher [42, 43] than the SM prediction

$$a_\mu^{\rm exp} - a_\mu^{\rm SM} = 288(80)\times 10^{-11}. \quad (27)$$

This result may signal the existence of new physics beyond the SM. New light (with a mass $m_{Z'} \le O(1)$ GeV) vector boson (dark photon) which couples very weakly with muon with $\alpha_{Z'} \sim O(10^{-8})$ can explain $g_\mu - 2$ anomaly [22–25]. Vector-like interaction of Z' boson with muon

$$L_{Z'} = g'\bar{\mu}\gamma^\nu\mu Z'_\nu \quad (28)$$

leads to additional contribution to muon anomalous magnetic moment [43]

$$\Delta a = \frac{\alpha'}{2\pi}F\left(\frac{m_{Z'}}{m_\mu}\right), \quad (29)$$

where

$$F(x) = \int_0^1 dz\frac{[2z(1-z)^2]}{[(1-z)^2 + x^2 z]}, \quad (30)$$

and $\alpha' = \dfrac{(g')^2}{4\pi}$. The relations (29, 30) allow to determine the coupling constant α' which explains the value (27) of muon anomaly. For $m_{Z'} \ll m_\mu$ one can find that

$$\alpha' = (1.8 \pm 0.5)\times 10^{-8}. \quad (31)$$

For another limiting case $m_{Z'} \gg m_\mu$ the α' is

$$\alpha' = (2.7 \pm 0.7)\times 10^{-8}\times\frac{m_{Z'}^2}{m_\mu^2}. \quad (32)$$

However the postulation of the interaction (28) is not the end of the story. The main question: what about the interaction of the Z' boson with other quarks and leptons? The renormalizable Z' interaction with the SM fermions ψ_k ($\psi_k = e, \nu_e, u, d, \ldots$) has the form

$$L_{Z'} = g' Z'_\mu J^\mu_{Z'}, \quad (33)$$

$$J^\mu_{Z'} = \sum_k [q_{Lk}\bar{\psi}_{Lk}\gamma^\mu\psi_{Lk} + q_{Rk}\bar{\psi}_{Rk}\gamma^\mu\psi_{Rk}], \quad (34)$$

where $\psi_{Lk,Rk} = \dfrac{1}{2}(1 \mp \gamma_5)\psi_k$ and q_{Lk}, q_{Rk} are the Z' charges of the ψ_{Lk}, ψ_{Rk} fermions. The Z' can interact

with new hypothetical particles beyond the SM, for instance, with DM fermions χ

$$L_{Z',\chi} = g_D Z'_\mu \bar{\chi}\gamma^\mu \chi. \quad (35)$$

There are several models of the current $J^\mu_{Z'}$. In a model with dark photon [13] Z' boson interacts with photon A_μ due to kinetic mixing term[5]

$$L_{mix} = -\frac{\epsilon}{2} F^{\mu\nu} Z'_{\mu\nu}. \quad (36)$$

As a result of the mixing (36) the field Z' interacts with the SM electromagnetic field $J^\mu_{EM} = \frac{2}{3}\bar{u}\gamma^\mu u - \frac{1}{3}\bar{d}\gamma^\mu d - \bar{e}\gamma^\mu e + \ldots$ with the coupling constant $g' = \epsilon e$ ($\alpha = \frac{e^2}{4\pi} = \frac{1}{137}$). However experimental data exclude dark photon model as an explanation of muon $g_\mu - 2$ anomaly. Other interesting scenario is the model [6] where Z' (the dark leptonic gauge boson) interacts with the SM leptonic current, namely

$$L_{Z'} = g'[\bar{e}\gamma^\nu e + \bar{\nu}_{eL}\gamma^\nu \nu_{eL} + \bar{\mu}\gamma^\nu \mu + \bar{\nu}_{\mu L}\gamma^\nu \nu_{\mu L} + \bar{\tau}\gamma^\nu \tau + \bar{\nu}_{\tau L}\gamma^\nu \nu_{\tau L}]Z'_\nu. \quad (37)$$

In refs. [22–24] for an explanation of $g_\mu - 2$ muon anomaly a model where Z' interacts predominantly with the second and third generations through the $L_\mu - L_\tau$ current

$$L_{Z'} = g'[\bar{\mu}\gamma^\nu \mu + \bar{\nu}_{\mu L}\gamma^\nu \nu_{\mu L} - \bar{\tau}\gamma^\nu \tau - \bar{\nu}_{\tau L}\gamma^\nu \nu_{\tau L}]Z'_\nu \quad (38)$$

has been proposed. The interaction (38) is γ_5-anomaly free, it commutes with the SM gauge group and moreover it escapes (see next section) from the most restrictive current experimental bounds because the interaction (38) does not contain quarks and first generation leptons ν_e, e. In ref. [44] a model where Z' couples with a right-handed current of the first and second generation SM fermions including the right-handed neutrinos has been suggested. The model is able to explain the muon $g_\mu - 2$ anomaly due to existence of light scalar and it can be tested in future experiments.

The Yukawa interaction of the scalar field with muon

$$L_{Yuk,\phi} = -g_{\mu\phi}\phi\bar{\mu}\mu. \quad (39)$$

leads to additional one loop contribution to muon anomalous magnetic moment [43]

$$\Delta a_\mu = \frac{g^2_{\mu\phi}}{8\pi^2}\frac{m^2_\mu}{m^2_\phi}\int_0^1 \frac{x^2(2-x)dx}{(1-x)(1-\lambda^2 x) + \lambda^2 x}, \quad (40)$$

where $\lambda = \frac{m_\mu}{m_\phi}$. For heavy scalar $m_\phi \gg m_\mu$

$$\Delta a_\mu = \frac{g^2_{\mu\varphi}}{4\pi^2}\frac{m^2_\mu}{m^2_\phi}\left[\ln\left(\frac{m_\phi}{m_\mu}\right) - \frac{7}{12}\right], \quad (41)$$

and for light scalar $m_\mu \gg m_\phi$

$$\Delta a_\mu = \frac{3g^2_{\mu\phi}}{16\pi^2}. \quad (42)$$

2.5.1. LDM and Z' boson interacting with $L_\mu - L_\tau$ current [27–30]. It is interesting that an extension of the $L_\mu - L_\tau$ model is able to explain today DM density in the Universe. Consider as an example the simplest extension with complex scalar LDM χ[6]. The interaction of the DM χ with the Z' boson is described by the Lagrangian

$$L_{\chi Z'} = (\partial^\mu \chi - ie_d Z'^\mu \chi)^*(\partial_\mu \chi - ie_d Z'_\mu \chi) - m^2_\chi \chi^*\chi - \lambda_\chi(\chi^*\chi)^2. \quad (43)$$

The nonrelativistic annihilation cross section $\chi\bar{\chi} \to \nu_\mu\bar{\nu}_\mu, \nu_\tau\bar{\nu}_\tau$ for $s \approx 4m^2_\chi$ has the form[7]

$$\sigma v_{rel} = \frac{8\pi}{3}\frac{\epsilon^2\alpha\alpha_D m^2_\chi v^2_{rel}}{(m^2_{Z'} - 4m^2_\chi)^2}. \quad (44)$$

We use standard assumption that in the hot early Universe DM is in equilibrium with ordinary matter. Using the formulae of Appendix A one can find that

$$\epsilon^2\alpha_D = k(m_\chi)\times 10^{-6}\times\left(\frac{m_\chi}{\text{GeV}}\right)^2\times\left[\frac{m^2_{Z'}}{m^2_\chi} - 4\right]^2. \quad (45)$$

Here the coefficient $k(m_\chi)$ depends logarithmically on DM mass m_χ and $k_{DM} \sim O(1)$ for 1 MeV $\le m_\chi \le$ 300 MeV.

As a consequence of (45) we find that for $m_{Z'} \ll m_\mu$ the values $\epsilon^2 = (2.5 \pm 0.7)\times 10^{-6}$ and

$$\alpha_D \sim 0.4k(m_\chi)\times\left(\frac{m_\chi}{\text{GeV}}\right)^2\times\left[\frac{m^2_{A'}}{m^2_\chi} - 4\right]^2 \quad (46)$$

[5] Here $F_{\mu\nu} = \partial_\mu A_\nu - \partial_\nu A_\mu$ and $Z'_{\mu\nu} = \partial_\mu Z'_\mu - \partial_\nu Z'_\mu$.

[6] The annihilation cross-section for scalar DM has p-wave suppressions that allows to escape CMB bound [74].

[7] Here we consider the case $m_{Z'} > 2m_\chi$.

explain both the $g_\mu - 2$ muon anomaly and today DM density.

3. CURRENT EXPERIMENTAL BOUNDS

3.1. The Reactions Used for the Search for LDM

Here we briefly describe the most interesting reactions used(or will be used) for the search for both visible and invisible A' decays at accelerators.

3.1.1. Visible A' decays searches. There are a lot of dark photon searches based on the use of visible A' decays $A' \to e^+e^-, \mu^+\mu^-$. The production mechanisms are $e^+e^- \to \gamma A'$, $eZ \to eZA'$ reactions, neutral meson decays $pZ \to (\pi^0/\eta^0 \to A'\gamma) + ...$ in proton nuclei collisions or direct A' production in proton nuclei reactions [4]. The A' boson is reconstructed as a narrow resonance. Also vertex detection for $A' \to l^+l^-$ decay can be used. Really, the A' decay length is proportional to $(\epsilon^2 m_{A'})^{-1}$ implying that searches for displaced vertices probe low values of the ϵ-parameter. Typical example is NA64 experiment.

3.1.2. Invisible A' decays. The DM is produced in the reactions like $eZ \to eZ(A' \to \chi\bar{\chi})$ or $e^+e^- \to \gamma(A' \to \chi\bar{\chi})$ and identified through the missing energy carried away by the escaping DM particles. The hermeticity of the detector is crusial for background rejection. Resonance hunt in missing mass distribution is very effective for the search for A' invisible decays. For instance, BaBar collaboration [45] used the reaction $e^+e^- \to \gamma(A' \to \chi\bar{\chi})$. The e^+, e^- and γ momenta are measured with good accuracy $O(10^{-2})$ that allows to restore the missing mass $m_{\text{mis}} = \sqrt{(p_{e^+} + p_{e^-} - p_\gamma)^2}$. The A' is searched for as a peak in distribution of the missing mass m_{mis}.

However there are experiments where the exact measurement of the initial and final particle momenta is impossible. For instance, the NA64 experiment [31] uses the reaction $eZ \to eZ(A' \to \chi\bar{\chi})$ for the search for A' invisible decays and measures only initial and final electron energies. The typical signature for the LDM detection is missing energy in electromagnetic calorimeter without essential activity in hadronic calorimeter. Good hermeticity of the detector allows to suppress the background at the level $O(10^{-11})$ or even less that is crusial for the A' detection. The number of signal events at NA64 is proportional to ϵ^2.

3.1.3. Electron and proton beam dump experiments. In beam dump experiments DM is produced in decays $\pi^0/\eta^{(\prime)} \to \gamma(A' \to \chi\bar{\chi})$ or in the reactions $pZ \to pZ(A' \to \chi\bar{\chi})$, $eZ \to eZ(A' \to \chi\bar{\chi})$ and it is detected via reactions $e\chi \to e\chi$, $N\chi \to N\chi$ in downstream detectors [4]. These experiments probe LDM twice and they are sensitive to LDM coupling constant $\alpha_D = \frac{e_D^2}{4\pi}$ with dark mediator A'. The number of events is proportional to $\epsilon^4\alpha_D$. Therefore a large proton(electron) flux is required.

3.2. Bound From Electron Magnetic Moment

The experimental and theoretical values for electron magnetic moment coincide at the 2.4σ level [46]

$$\Delta a_e \equiv a_e^{\text{exp}} - a_e^{\text{SM}} = -(0.87 \pm 0.36) \times 10^{-12}. \quad (47)$$

The A' boson contributes to the Δa_e at one loop level, see formulae (40)–(42). From the value (47) of Δa_e it is possible to restrict the couplng constants g_{Ve} and g_{Ae}. For the model with equal muon and electron vector couplings $g_{Ve} = g_{V\mu}$ and $g_{Ae} = g_{A\mu} = 0$ the $g_\mu - 2$ muon anomaly explanation is excluded for $M_{A'} \le 20$ MeV [47].

3.3. Visible A' Decays

3.3.1. Fixed target electron experiments. Fixed target experiments APEX [48] and A1 at MAMI(Mainz Microtron) [49] searched for A' in electron-nucleus scatterings using the A' bremsstrahlung production $e^-Z \to e^-ZA'$ and subsequent A' decay into electron-positron pair $A' \to e^+e^-$. The absence of the resonance peak in the invariant e^+e^- mass spectrum allows to obtain upper limits on the A' boson coupling constants g_{Ve}, g_{Ae} of the A' with electron, see Fig. 1. The A1 collaboration excluded the masses $50\ \text{MeV} < M_{A'} < 300\ \text{MeV}$ [49] for $g_\mu - 2$ muon anomaly explanation in the model with equal muon and electon couplings of the A' boson with a sensitivity to the mixing parameter up to $\epsilon^2 = 8 \times 10^{-7}$. APEX collaboration used ~2 GeV electron beam at Jefferson Laboratory and excluded masses $175\ \text{MeV} < M_{A'} < 250\ \text{MeV}$ for $g_\mu - 2$ muon anomaly explanation in the model with equal muon and electon couplings of the A' boson. Recently NA64 collaboration studied long lived $A' \to e^+e^-$ decays and obtained new bounds on mixing parameter ϵ, see sect. 4.

3.3.2. e^+e^- experiments. Bar experiment has constrained visible A' decays by using $\Upsilon(1S)$ decays BaBar collaboration [50] looked for visible decays of light A' bosons in the reaction $e^+e^- \to \gamma A'$, $A' \to l^+l^-(l = e, \mu)$

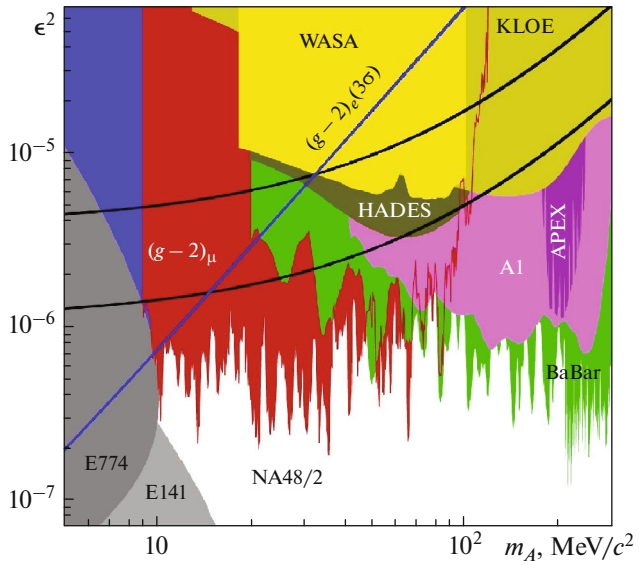

Fig. 1. Current limits at 90% CL on the mixing parameter ϵ^2 versus the A' mass for visible A' decays, taken from ref. [52].

as resonances in the l^+l^- spectrum. For the model with the A' dark photon the mixing strength values 10^{-2}–10^{-3} are excluded for 0.212 GeV $< m_{A'} <$ 10 GeV [50] in the assumption that visible A' decays into the SM particles dominate, see Fig. 1. The KLOE experiment at the DAΦNE Φ-factory in Fraskati searched for A' in decays $\Phi \to \eta A' \to \eta e^+e^-$ and $\Phi \to \gamma(A' \to \mu^+\mu^-)$ [51]. The obtained bounds are weaker than those from NA48/2 [52] and MAMI [49] bounds.

Recently BaBar collaboration used the reaction $e^+e^- \to Z'\mu^+\mu^-, Z' \to \mu^+\mu^-$ to search for the Z' boson coupled with muon. The use of this process allows to restrict directly the muon coupling $g_{V\mu}$ of the Z' boson. The obtained results exclude the model with $L_\mu - L_\tau$ interaction as possible explanation of $g_\mu - 2$ muon anomaly for $m_{Z'} > 214$ MeV [53].

3.3.3. Fixed target proton experiments. The NA-48/2 experiment used simultaneous K^+ and K^- secondary beams produced by 400 GeV primary CERN SPS protons for the search for light A' boson in π^0 decays [52]. The decays $K^\pm \to \pi^\pm\pi^0$ and $K^\pm \to \pi^0\mu^\pm\nu$ have been used to obtain tagged π^0 mesons. The decays $\pi^0 \to \gamma A'$, $A' \to e^+e^-$ have been used for the search for A' boson. The A' boson manifests itself as a narrow peak in the distribution of the e^+e^- invariant mass spectrum. For the model with dark photon the obtained bounds exclude the $g_\mu - 2$ muon anomaly explanation for A' boson masses 9 MeV $< m_{A'} <$ 70 MeV [52], see Fig. 1. It should be noted that the decay width $\pi^0 \to \gamma A'$ is proportional to $(g_{Vu}q_u - g_{Vd}q_d)^2 = (2g_{Vu} + g_{Vd})^2/9$ and for the models with nonuniversal A'-boson couplings[8], for instance, for the model with $L_\mu - L_\tau$ interaction current the NA-48/2 bound [52] is not applicable.

3.3.4. ATLAS and CMS bounds on light particles in Higgs boson decays. ATLAS collaboration searched for new light particles γ_d in Higgs boson decays $h \to 2\gamma_d + X$, $h \to 4\gamma_d + X$ [55]. In the assumption that new boson γ_d decays mainly into muon pair bounds on $\mathrm{Br}(h \to 2\gamma_d + X)$ and $\mathrm{Br}(h \to 4\gamma_d + X)$ have been otained [55]. It should be stressed that for the model with dark photon the bound on ϵ parameter is rather weak.

CMS collaboration also searched for new particles [56] in the Higgs boson decay $h \to 2a + X \to 4\mu + X$. Bounds similar to the ATLAS bounds have been obtained.

3.3.5. LHCb bound on $A' \to \mu^+\mu^-$ decays. Recently LHCb collaboration performed the search for A' bosons on the base of visible $A' \to \mu^+\mu^-$ decay. In the assumption that the A' production arises as a result of $\gamma A'$ mixing the bound on mixing parameter ϵ has been derived for wide range of A' masses from 214 MeV up to 70 GeV for prompt decays and for 214 MeV $< m_{A'} <$ 350 MeV for long lived A' [57]. No evidence for signal has been found and upper bound on ϵ parameter has been derived. The obtained bounds are the most stringent to date for the masses 10.6 GeV $< m_{A'} <$ 70 GeV.

3.4. Invisible A' Decays

3.4.1. Constraints from $K \to \pi$ + nothing decay. Light vector boson A' can be produced in the $K \to \pi A'$ decay in the analogy with the SM decay $K \to \pi\gamma^*$ of K-meson into pion and virtual photon. For the model with the dominant A' decay into invisible modes nontrivial bound on the A' boson mass and the coupling constant arises. Namely, the results of BNL E949 and E787 experiments [58] on the measurement of the $K^+ \to \pi^+\nu\bar{\nu}$ decay width were used to obtain an upper bound on the $\mathrm{Br}(K^+ \to \pi^+A')$ decay

[8] In ref. [54] models with $2g_{Vu} + g_{Vd} \approx 0$ have been suggested for an explanation of recent discovery claim [26] of 17 MeV narrow resonance observed as a peak in e^+e^- invariant mass distribution in nuclear transitions.

as a function of the A' mass in the assumption that $A' \to$ invisible decay dominates. In the model where the A' is dark photon, the explanation of muon $g_\mu - 2$ anomaly due to the A' existence is excluded for $M_{A'} > 50$ MeV except the narrow region around $m_{A'} = m_\pi$ [59–61]. Note that in models with non-electromagnetic current interactions of A' with quarks and leptons, for instance, in the model where the A' interacts with the $L_\mu - L_\tau$ current only, the bound from $K \to \pi +$ nothing decay does not work or it is rather weak [60].

3.4.2. The use of the reaction $eZ \to eZA'$, $A' \to$ invisible. The NA64 collaboration [32, 33] used the reaction $eZ \to eZA'$, $A' \to$ invisible for the search for invisible dark photon decays into LDM particles. The obtained bounds exclude the dark photon model as an explanation of muon $g_\mu - 2$, see Fig. 2.

3.4.3. e^+e^- experiments. Recently BaBar collaboration [62] used the reaction $e^+e^- \to \gamma A'$, $A' \to$ invisible for the search for invisible decays of A'. In the assumption that A' invisible decays dominate the bound $\epsilon \le 10^{-3}$ has been obtained for $m_{A'} \le 9.5$ GeV, see Fig. 2.

3.4.4. Electron beam dump experimemts. In electron beam dump experiments the reaction $eZ \to eZA'$ is used for the A' production. After some shield the A' bosons are manifested as visible decays $A' \to e^+e^-, \mu^+\mu^-$. If A' decays mainly into LDM particles $A' \to \chi\bar{\chi}$ the use of elastic scattering $\chi e \to \chi e$, $\chi N \to \chi N$ in the far detector allows to detect LDM particles. The results of electron beam dump experiments [63, 64] at SLAC and FNAL have been used [65] to constrain the couplings of light gauge boson A'. For the case of dominant A' decays into visible particles electron beam dump experiments exclude $10^{-7} \le \epsilon \le 10^{-6}$ for $m_{A'} \le 20$ MeV. For the case where the A' decays dominantly into LDM particles the experiment E137 gives the most stringent bounds and it excludes the parameter $y \equiv \epsilon^2 \alpha_D \left(\frac{m_\chi}{m_{A'}}\right)^4 \ge 10^{-11}(10^{-9})$ for $m_{A'} \le 1(100)$ MeV.

3.4.5. Proton beam dump experiments. In proton beam dump experiments the main source of the A' arises as a result of $\pi^0(\eta)$ production $pZ \to \pi^0(\eta) + ...$ with the subsequent $\pi^0(\eta) \to \gamma A'$; $A' \to e^+e^-$ decays, see e.g [66, 67]. In the case of dominant A' decay into LDM particles $A' \to \chi\bar{\chi}$ the reactions $\chi e \to \chi e$ and $\chi N \to \chi N$ are used for dark matter identification.

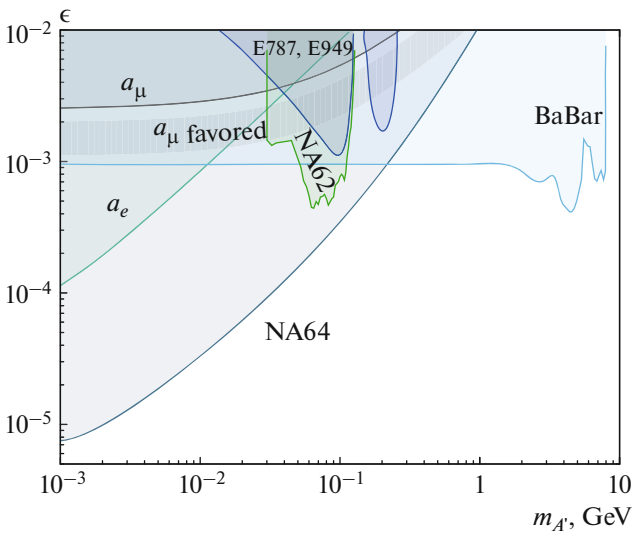

Fig. 2. Limits at 90% C.L. on the mixing parameter ϵ versus the A' mass for invisible A' decays, taken from ref. [34].

The LSND (Liquid Scintillarion Neutrino Detector) [68] at Los Alamos was constructed to detect neutrino. Neutrino arise mainly from the reaction $pZ \to \pi^+ + ...$ with the subsequent $\pi^+ \to \mu^+\nu_\mu$ decays. LSND data with $N = 10^{24}$ POT also allow to restrict the dark photon couplings. Dark photons A' are produced mainly in the reaction $pZ \to (\pi^0 \to \gamma A') + ...$ The LSND bound on the parameter $y \equiv \epsilon^2 \alpha_D \left(\frac{m_\chi}{m_{A'}}\right)^4$ is by factor $O(10)$ more strong that the corresponding bound from electron beam dump experiment E137. The MiniBoone experiment at FNAL is also proton beam dump experiment which uses the FNAL 8 GeV Booster proton beam. As in LSND dark photons are produced mainly in π^0 decays and detected in a 800 tonn mineral oil Cherenkov detector situated ~500 m downstream of the beam dump. Recently MiniBoone experiment has obtained bound [69] on $y \le 10^{-8}$ for $\alpha_D = 0.5$ and for DM masses $0.01 < m_\chi < 0.3$ GeV in a dedicated run with 1.86×10^{20} protons delivered to a steel beam dump.

3.4.6. COHERENT at ORNL. The primary goal of the COHERENT experiment [70] at Oak Ridge National Laboratory(USA) is to measure coherent elastic neutrino scattering ($CE\nu NS$) process and to check the N^2 dependence of the cross section.

Recently the COHERENT experiment measured the $CE\nu NS$ process [71] and the results are in agreement with the SM expectations. The COHERENT is beam-dump experiment and LDM can be produced mainly in $\pi^0 \to \gamma A' \to \gamma\chi\bar{\chi}$ decays. DM particles scatter in scintillating cristals and liquid argon detectors at the Apallation Neutron Source at ORNL. The DM particles(if they exist) are produced via $\pi^0/\eta \to \gamma A'$ decays and they can be identified through coherent scattering leading to detectable nuclear recoil. In ref. [72] recent COHERENT data [71] have been used for the derivation of the bounds for LDM. For $1 < m_\chi < 90$ MeV the bound on $\epsilon e_d^{1/2}$ is between 10^{-5} and 10^{-4}.

3.5. Bound from the Neutrino Trident Process

$$\nu_\mu N \to \nu_\mu N \mu^+ \mu^-$$

The neutrino trident $\nu_\mu N \to \nu_\mu N \mu^+ \mu^-$ events allow to restrict a model where Z' boson interacts with $L_\mu - L_\tau$ current. The data of the CHARM and the CCFR experiments exclude the $g_\mu - 2$ muon anomaly explanation for $m_{Z'} \geq 400$ MeV [73].

3.6. Nonaccelerator Bounds

3.6.1. CMB bound. The residual annihilation of DM particles after equilibrium annihilation and before recombination can still reionize hydrogen and hence modify the CMB (cosmic microwave background) power spectrum. The Planck experiment constraint [74] rules out thermal DM below 10 GeV if the annihilation is s-wave (velocity independent). The p-wave annihilation is allowed since at recombination epoch the temperature is $T \sim$ eV and the p-wave annihilation is suppressed by factor T/m_χ. Also models with pseudo-Dirac LDM [4, 37] escape the CMB bound.

3.6.2. Constraints from stars. Light A' boson can be produced in stars. The energy loss of the stars through the A' places strong limits $\epsilon \leq O(10^{-14})$ on the A' couplings for $m_{A'} \leq 0.01$ MeV [75–83]. The constraints on the A' couplings result from the requirement that the energy loss by the A' emission has to be less than 10 percent of the solar energy in photons [76]. Also for $m_{A'} \leq 0.3$ MeV similar but more weak limit on ϵ can be derived from horizontal branch stars and red giants where the temperatures are higher than in the Sun [76].

3.6.3. Supernnova 1987A bounds. Bounds from Supenova 1987A are based on the fact that if dark photons are produced in sufficient quantity, they reduce the amount of energy emitted in the form of neutrinos, in conflict with observations. In ref. [77] bounds on ϵ parameter were obtained for the model with dark photon. Bounds on ϵ parameter exist for $m_{A'} \leq 120$ MeV [77]. For the most interesting case $m_{A'} \geq 2m_e$ the value $\epsilon \geq O(10^{-7})$ does not contradict to data drom Supernova 1987A [77]. It means that the bounds from Supernova 1987A don't restrict severely the LDM hypothesis.

3.6.4. Constraints from BBN. Big Bang nucleosynthesis (BBN) can also provide the constraints on A' coupling constants. During the first several minutes after the Big Bang, the temperature of the Universe rapidly decreased as a consequence of the Universe expansion. During the Universe expansion some light elements are produced and the predictions of their abundance from BBN agree with experimental data [78]. The constraints on new interactions are based on the fact that new relativistic particle increases the expansion rate of the Universe through an additional degree of freedom which usually expressed in terms of extra neutrinos ΔN_ν. The larger Universe expansion rate increases the freeze-out temperature, therefore the n/p ratio and as a consequence the ^{4}He abundance is increased. The observed value of the ^{4}He abundance leads to the bound on ΔN_ν that is equivalent to the bounds on coupling constants of new relativistic particle. For dark photon model BBN constraints have been obtained in ref. [81]. The A' dark photon model with $m_{A'} \leq O(1)$ MeV is excluded [79] as a mediator explaining current DM abundance. Note that in ref. [82] lower bound $m_\chi \geq O(1)$ MeV on the mass of the LDM particle was obtained from the experimental bound on effective number of neutrinos.

3.7. Direct LDM Detection

The main problem of the LDM detection via elactic LDM scattering at nuclei is the size of the nuclear recoil energy [4]. The velocity of DM is $v_\chi \sim 10^{-3}$ s and the maximum possible energy transfer is proportional to the square of the reduced mass $\mu_{\text{red}} = \dfrac{m_{\text{nuclei}} m_\chi}{m_{\text{nuclei}} + m_\chi}$. The nuclear recoil energy is [4]

$$E_{\text{NR}} = \frac{q^2}{2m_{\text{nuclei}}} \leq \frac{2\mu_{\text{red}}^2 v_\chi^2}{m_{\text{nuclei}}} \leq 190 \text{ eV} \times \left(\frac{m_\chi}{500 \text{ MeV}}\right)^2 \times \left(\frac{16 \text{ GeV}}{m_{\text{nuclei}}}\right) \quad (48)$$

that makes the detection of LDM with masses $m_\chi \leq O(1)$ GeV at nuclei extremely difficult. The remaining possibility is the use of electron LDM elas-

tic scattering [4]. For electron LDM scattering the maximum energy transfer to electron is

$$E_e \le \frac{1}{2} m_\chi v_\chi^2 \le 3 \text{ eV} \left(\frac{m_\chi}{\text{MeV}}\right). \quad (49)$$

Bound electrons with binding energy ΔE_B can produce measurable signal at [4]

$$m_\chi \ge 0.3 \text{ MeV} \times \left(\frac{\Delta E_B}{1 \text{ eV}}\right). \quad (50)$$

The elasic nonrelativistic cross-section of scalar or fermion LDM in dark photon model at $m_\chi \gg m_e$ is [4, 84]

$$\sigma(e\chi \to e\chi) = \frac{16\pi m_e^2 \alpha \epsilon^2 \alpha_D}{(m_{A'}^4)}, \quad (51)$$

while the elastic Majorana cross-section is suppressed by factor $k_M = \frac{2m_e^2}{m_\chi^2} v_\chi^2$

$$\sigma(e\chi_{\text{Majorana}} \to e\chi_{\text{Majorana}}) = \frac{16\pi m_e^2 \alpha \epsilon^2 \alpha_D}{(m_{A'}^4)} \times k_M \quad (52)$$

that makes the direct detection of Majorana LDM in dark photon model extremely difficult or even hopeless.

Recently XENON1T collaboration has published new record results [85] on the search for direct electron LDM scattering. New bounds on elasic electron LDM cross sections were obtained for $m_\chi \ge 30$ MeV. For the model with dark photon the use of the formula (51) and the results of ref. [85] allows to derive bound on $\epsilon^2 \alpha_D$. In Fig. 3 the comparison of 90% C.L. upper limits on the cross-sections of LDM electron scattering transmitted by dark photon mediator A' calculated by using NA64 [34] and BaBar bounds and the XENON1T [85] bounds has been presented for $\alpha_D = 0.1$. For $m_\chi \le 50$ MeV the NA64 bound is stronger than the XENON1T bound. For pseudo-Dirac fermions with not too small $\delta = \frac{m_{\chi_2} - m_{\chi_1}}{m_{\chi_1}}$ the reaction of χ_2 electroproduction $\chi_1 e \to \chi_2 e$ for nonrelativistic LDM χ_1 is prohibited due to energy conservation law, while elastic $\chi_1 e \to \chi_1 e$ scattering is absent at tree level that extremely complicates the direct LDM detection for pseudo-Dirac fermions.

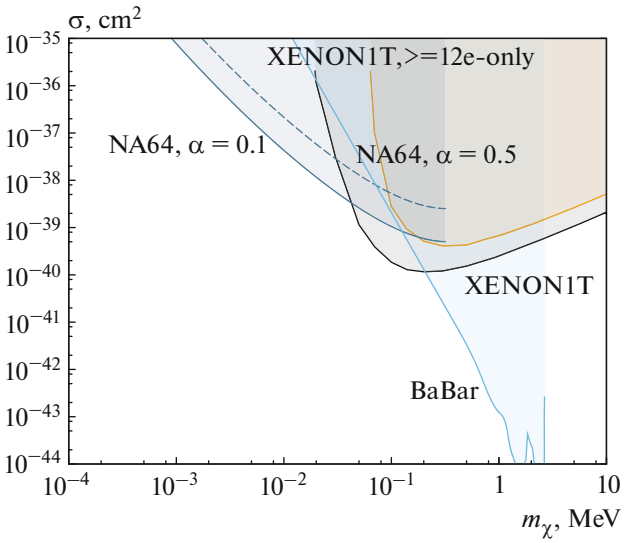

Fig. 3. Comparison of 90% C.L. upper limits on LDM-electron scattering cross-sections calculated by using NA64 [34] and BaBar constraints on kinetic-mixing from Fig. 2 with results of direct searches by XENON1T [85]. The blue curves are calculated for $\alpha_D = 0.1$, while the dashed blue for $\alpha_D = 0.5$. The Yellow dashed line shows the XENON1T limit obtained without considering signals with <12 produced electrons.

4. NA64 EXPERIMENT

4.1. Invisible Mode

NA64 experiment [31] at the CERN SPS employs the electron beam from the H4 beam line in the North Area (NA). The beam delivers $\approx 5 \times 10^6 e^-$ per SPS spill of 44.8*s* produced by the primary 400 GeV proton beam with an intensity of a few 10^{12} protons on target. The NA64 experiment is a fixed target experiment searching for dark sector particles at the CERN Super Proton Synchrotron(SPS) by using active beam dump technique combined with missing energy approach [31, 86–88]. If new light boson A' exists it could be produced in the reaction of high energy electrons scattering off nuclei. Compared to the traditional beam dump experiment the main advantage of the NA64 experiment is that its sensitivity is proportional to the ϵ^2. While for the classical beam dump experiments the sensitivity is proportional to the $\epsilon^2 \cdot \epsilon^2$, where one ϵ^2 comes from new particle production in the dump and another ϵ^2 is from the LDM interaction in far detector. Another advantage of the NA64 experiment is that due to the higher energy of the incident beam, the centre-of-mass system is boosted relative to the laboratory system. This boost leads to enhanced hermeticity of the detector providing a nearly full solid angle coverage.

The NA64 method of the search can be illustrated by considering the search for the dark photon A' production for invisible A' decays $A' \to \chi\bar{\chi}$ into LDM particles. A fraction f of the primary beam energy $E_{A'} = fE_0$ is carried away by χ LDM particles, which penetrate the target and detector without interactions resulting in zero energy deposition. The remaining part of beam energy $E_e = (1 - f)E_0$ is deposited in the

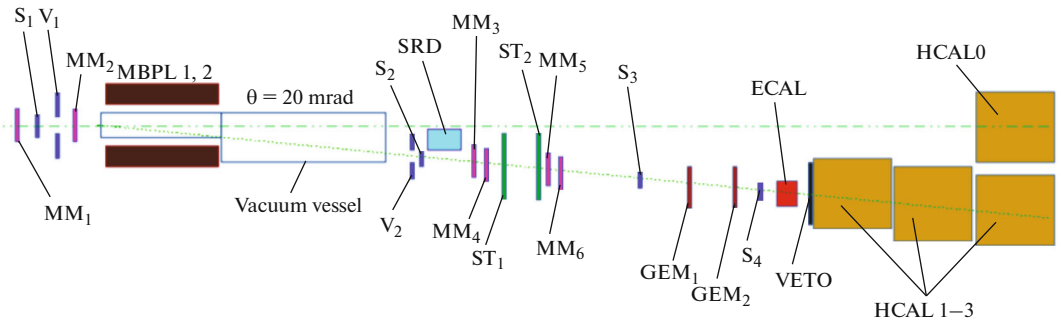

Fig. 4. Schematic illustration of the setup to search for invisible decays of the bremsstrahlung A's produced in the reaction $eZ \to eZA'$ of 100 GeV e^- incident on the active ECAL target.

target by the scattered electron. The occurrence of the A' production via the reaction $eZ \to eZA'$; $A' \to \chi\bar{\chi}$ would appear as an excess of events with a signature of a single isolated electromagnetic (e-m) shower in the active dump with energy E_e accompanied by a missing energy $E_{\text{miss}} = E_{A'} = E_0 - E_e$ above those expected from backgrounds. Here we assume that LDM particles χ traverse the detector without decaying visibly. Currently, the NA64 employs the 100 GeV electron beam from $H4$ beam line at the North Area (NA) of the CERN SPS. The beam was optimized to transport the electrons with the maximal intensity $\geq 10^7$ per SPS spill with the momentum 100 GeV/c. The NA64 detector is schematically shown in Fig. 4. The setup utilized the beam defining scintillator (Sc) counters $S1$–$S3$ and veto V1, and the spectrometer consisting of two successive dipole magnets with the integral magnetic field of $\approx 7T \times m$ and low-material-budget tracker. The tracker is a set of upstream Micromegas chambers $(T1, T2)$ and downstream Micromegas, GEM and Straw tube stations, measuring the beam e^- momenta, P_e with the precision $\delta P_e/P_e \approx 10^{-2}$ [31]. The magnets also serve as an effective filter rejecting the low energy electrons present in the beam. The key feature of NA64 is the use of synchrotron radiation (SR) from high energy electrons in the magnetic field to significantly enhance electron identification and suppress background from a hadron contamination in the beam. A 16 m long vacuum vessel was installed between the magnets and the ECAL to minimize absorption of the SR photons detected immediately at the downstream end of the vessel with a SRD, which is array of PbSc sandwich counters of a very fine longitudinal segmentation assembled from 80–100 μm Pb and 1 mm Sc plates with wave length shifting (WLS) fiber read-out. This allowed to additionally suppress background from hadrons, that could knock off electrons from the output vacuum window of the vessel producing a fake $e^- SRD$ tag, by about two orders of magnitude. The detector is also equipped with an active target, which is a hodoscopic electromagnetic calorimeter (ECAL) for the measurement of the electron energy deposition, E_{ECAL}, with the accuracy $\delta E_{\text{ECAL}}/E_{\text{ECAL}} \approx 0.1/\sqrt{E_{\text{ECAL}}\ [\text{GeV}]}$ as well as the X, Y coordinates of the incoming electrons by using the transverse $e-m$ shower profile. The ECAL is a matrix of 6×6 Shashlik-type counters assembled with Pb and Sc plates with WLS fiber read-out. Each model is $\approx$40 radiation lengths (X_0) and has an initial part $\approx 4X_0$ used as a preshower (PS) detector. By requiring the presence of in-time SR signal in all three SRD counters, and using the information of the longitudinal and lateral shower development in the ECAL, the initial level of the hadron contamination in the beam $\pi/e^- \leq 10^{-2}$ was further suppressed by more than 4 orders of magnitude, while the electron ID at the level $\geq$95%. A high-efficiency veto counter *Veto*, and a massive, hermetic hadronic calorimeter (HCAL) of $\approx$ 30 nuclear interaction lengths (λ_{int}) were positioned after the ECAL. The *Veto* is a plane of scintillation counters used to veto charged secondaries incident on the HCAL detectors from upstream e^- interactions. The HCAL which was an assembly of four modules HCAL0–HCAL3 served as an efficient veto to detect muons of hadronic secondaries produced of in the $e^- A$ interactions ECAL target. The HCAL energy resolution is $\delta E_{\text{HCAL}}/E_{\text{HCAL}} \approx 0.6/\sqrt{E_{\text{HCAL}}\ [\text{GeV}]}$.

4.2. Visible Mode

The NA64 setup designed for the searches for decays $X, A' \to e^+e^-$ of the X bosons, which could explain the ^{8}Be anomaly (see below 5.1.2) and the A' is schematically shown in Fig. 5. The NA64 experiment for visible $A' \to e^-e^+$ searches employs the optimized electron beam from the H4 beam line in the North Area (NA) of the CERN SPS. The beam delivers

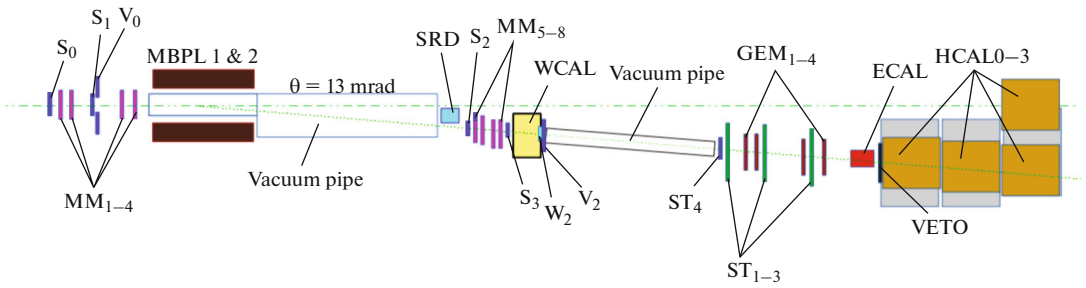

Fig. 5. Schematic illustration of the setup to search for visible $A', X \to e^+e^-$ decays decays of the bremsstrahlung A', X produced in the reaction $eZ \to eZA'$ of 100 GeV e^- incident on the active WCAL target.

5×10^6 EOT per SPS spill of 4.8s produced by the primary 400 GeV proton beam with an intensity of a few 10^{12} protons on target. Two scintillation counters, $S1$ and $S2$ were used for the beam definition, while the other two, $S3$ and $S4$, were used to detect the e^+e^- pairs. The detector is equipped with a magnetic spectrometer consisting of two MPBL magnets and a low material budget tracker. The tracker was a set of four upstream Micromegas (MM) chambers ($T1, T2$) for the incoming e- angle selection and two sets of downstream MM, GEM stations and scintillator hodoscopes ($T3, T4$) allowing the measurement of the outgoing tracks [31]. To enhance the electron identification the synchrotron radiation (SR) emitted by electrons was used for their effi- cient tagging and for additional suppression of the initial hadron contamination in the beam $\pi/e \times 10^{-2}$ down to the level 10^{-6} [87]. The use of SR detectors (SRD) is a key point for the hadron background suppression and improvement of the sensitivity compared to the previous electron beam dump searches [31]. The dump is a compact electromagnetic (e-m) calorimeter WCAL made as short as possible to maximize the sensitivity to short lifetimes while keeping the leakage of particles at a small level. The WCAL was assembled from the tungsten and plastic scintillator plates with wave lengths shifting fiber read-out. The first (last) few layers of the WCAL were read separately to form a signal from a preshower (veto W_2) counter. Immediately after the W_2 there is also one more veto counter $V2$, and several meters downstream the signal counter $S4$ and tracking detectors. These detectors are followed by another e-m calorimeter (ECAL), which is a matrix of 6 shashlik-type lead—plastic scintillator sandwich modules [89]. Downstream the ECAL the detector was equipped with a high-efficiency veto counter, and a thick hadron calorimeter (HCAL) [31] used as a hadron veto and muon identificator. For the cuts selection, calculation of various efficiencies and background estimation the package for the detailed full simulation of the experiment based on Geant4 [90] is developed. It contains the subpackage for the simulation of various types of DM particles based on the exact tree-level calculation of cross sections [40, 41]. The method of the search for $A' \to e^-e^+$ decays is described in [31]. The application of all further considerations to the case of the $X \to e^+e^-$ decay is straightforward. If the A' exists, it could be produced via the coupling to electrons wherein high energy electrons scatter off a nuclei of the active WCAL dump target, followed by the decay into e^+e^- pairs:

$$e^- + Z \to e^- + Z + A', \quad A' \to e^-e^+. \tag{53}$$

The reaction (53) typically occurs within the first few radiation lengths (X_0) of the WCAL. The downstream part of the WCAL serves as a dump to absorb completely the e-m shower tail. The bremsstrahlung A' would penetrate the rest of the dump and the veto counter $V2$ without interactions and decay in flight into an e^+e^- pair in the decay volume downstream the WCAL. A fraction (f) of the primary beam energy $E_1 = fE_0$ is deposited in the WCAL by the recoil electron from the reaction (51). The remaining part of the primary electron energy $E_2 = (1 - f)E_0$ is transmitted through the dump by the A', and deposited in the second downstream calorimeter ECAL via the $A' \to e^+e^-$ decay in flight. The occurrence of $A' \to e^+e^-$ decays produced in eZ interactions would appear as an excess of events with two e-m-like showers in the detector: one shower in the WCAL and another one in the $ECAL$, with the total energy $E_{\text{tot}} = E_{\text{WCAL}} + E_{\text{ECAL}}$ equal to the beam energy (E_0), above those expected from the background sources.

5. CURRENT AND FUTURE NA64 RESULTS

In this section we briefly discuss last NA64 results and the perspectives of the NA64e(future NA64 experiment with electron beam) and NA64μ (future NA64 experiment with muon beam).

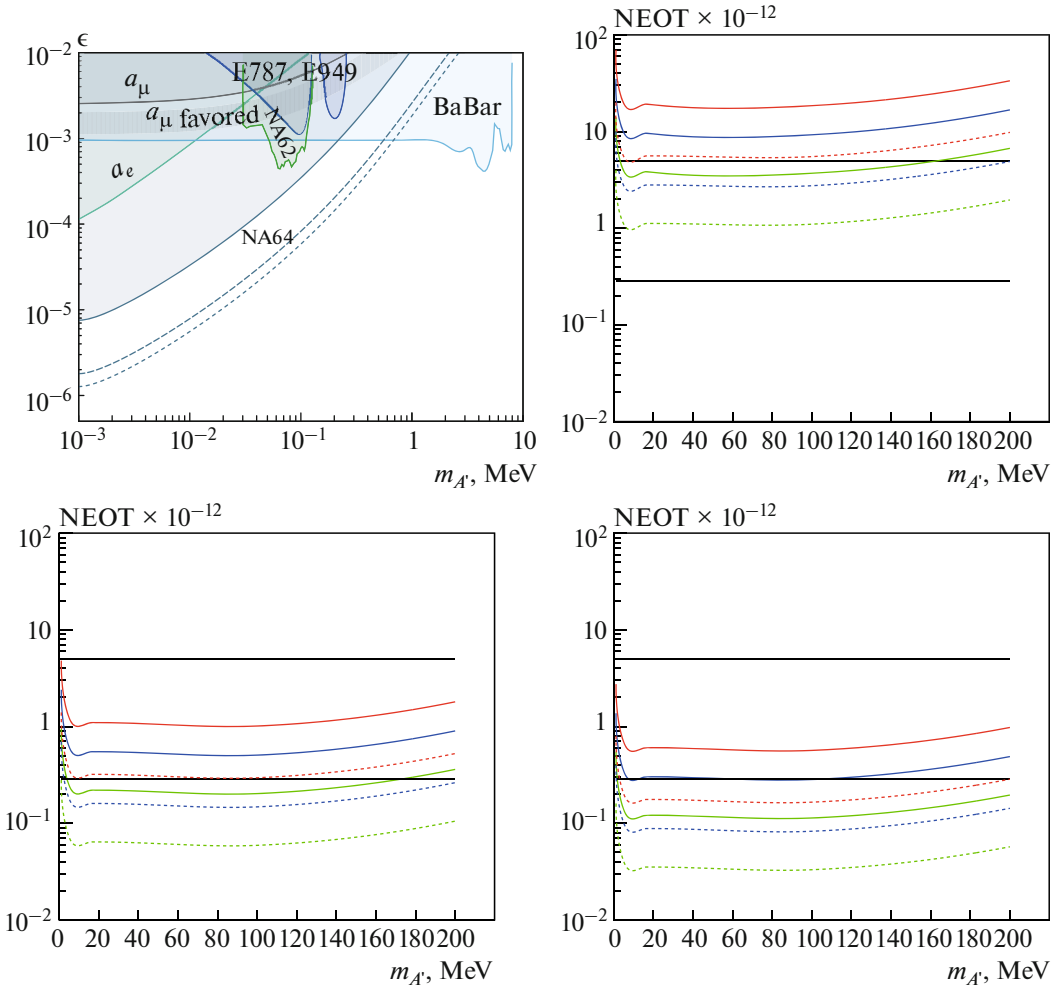

Fig. 6. The upper l.h.s. panel shows the NA64 90% C.L. current bound (solid) [34], and projected boundes for 5×10^{12}(dashed) and 10^{13} (dotted) in the $(m_{A'}, \epsilon^2)$ plane. The upper r.h.s plot and lower plots show the required number of EOT for the 90% C.L. exclusion of the A' with a given mass $m_{A'}$ in the $(m_{A'}, n_{\rm EOT}\times10^{-12})$ plane for pseudo-Dirac with $\delta \ll 1$ (the upper r.h.s panel), Majorana (the lower l.h.s. panel), and scalar (the lower r.h.s. panel) DM models for $\frac{m_{A'}}{m_\chi} = 2.5$ (solid), and = 3 (dashed), and $\alpha_D = 0.1$ (red), 0.05 (blue), and 0.02 (green). Upper(lower) black lines correspond to $n_{\rm EOT} = 5\times10^{12}(2.84\times10^{11})$. The curves under lower black line are excluded by last NA64 results [34].

5.1. NA64e

5.1.1. Invisible mode. Dark photon bounds. The NA64 collected NEOT = 2.84×10^{11} statistics in the 2016–2018 years. Recently NA64 collaboration [34] has been analyzed these data and obtained new bounds on ϵ parameter[9] by factor ~2.5 stronger the previous bound [32], see the upper l.h.s. panel in Fig. 6. After the long shutdown (LS2) at CERN the NA64 experiment plans to accumulate NEOT $\gtrsim 5\times10^{12}$. The NA64e future expected limits on mixing strength ϵ after the LS2 period assuming the zero-background case are shown in the upper l.h.s. panel in Fig. 6.

To estimate NA64 LDM discovery potential we have used the formulae of Appendix A to calculate the predicted value of ϵ^2 as a function of α_D, m_χ and $m_{A'}$, in the assumption that in the early Universe LDM was in thermo equilibrium. We used the values $\alpha_D = 0.02, 0.05, 0.1$ and $\frac{m_{A'}}{m_\chi} = 2.5, 3$. We have made the calculations for the case of scalar, Majorana and

[9] The assumption that Br($A' \to$ invisible) = 1 has been used.

pseudo-Dirac LDM with ($\delta \ll 1$). Our results [91] are presented in Fig. 6. The upper r.h.s plot and lower plots in Fig. 6 show the required number of EOT for the 90% C.L. exclusion of the A' with a given mass $m_{A'}$ in the $(m_{A'}, n_{\mathrm{EOT}} \times 10^{-12})$ plane for pseudo-Dirac with $\delta \ll 1$ (the upper r.h.s panel), Majorana (the lower l.h.s. panel), and scalar (the lower r.h.s. panel) LDM models for $\frac{m_{A'}}{m_\chi} = 2.5$ (solid), and = 3 (dashed), and $\alpha_{\mathrm{D}} = 0.1$ (red), 0.05 (blue), and 0.02 (green). We see that NA64 experiment has already excluded scalar LDM model with $\alpha_{\mathrm{D}} \le 0.1$, $\frac{m_{A'}}{m_\chi} \ge 3$ and Majorana LDM with $\alpha_{\mathrm{D}} = 0.02$, $\frac{m_{A'}}{m_\chi} \ge 2.5$. As one can see from Fig. 6 with $n_{\mathrm{EOT}} = 5 \times 10^{12}$ NA64e will be able to exclude the most interesting and natural LDM scenarios in the A' mass range 1 MeV $\le m_{A'} \le 150$ MeV except the most difficult case of pseudo-Dirac LDM with $\alpha_{\mathrm{D}} = 0.1$, $\alpha_D = 0.05$ and $\frac{m_{A'}}{m_\chi} = 2.5$.

5.1.2. The problem with resonance region. The expressions for the annihilation cross-sections are proportional to the factor $K = \epsilon^2 \alpha_{\mathrm{D}} \left(\frac{m_{A'}^4}{m_\chi^2} - 4 \right)^{-2}$. From the assumption that in the early Universe the LDM was in equilibrium with the SM matter we can predict the dependence of K on DM mass m_χ, see Appendix A. In the resonance region $m_{A'} \approx 2m_\chi$ the ε^2 parameter is proportional to K^{-1} that can reduce the predicted ϵ^2 value by (2–4) orders of magnitude [92] in comparison with the often used reference point $\frac{m_{A'}}{m_\chi} = 3$. It means that NA64 experiment and probably other future experiments will not be able to test the region $m_{A'} \approx 2m_\chi$ completely. It should be mentioned that the values of $m_{A'}$ and m_χ are arbitrary, so the case $m_{A'} = 2m_\chi$ could be considered as some fine-tuning. It is natural to require the absence of significant fine-tuning. We require that $\left(\frac{m_{A'}}{2m_\chi} - 1 \right) \ge 0.25$, i.e. $m_{A'} \ge 2.5 m_\chi$. In our estimates (see Fig. 6) we used two values $\frac{m_{A'}}{m_\chi} = 2.5$ and $\frac{m_{A'}}{m_\chi} = 3$. As it follows from the previous subsection the NA64 will be able to test the most interesting LDM models for the case of significant fine-tuning absence.

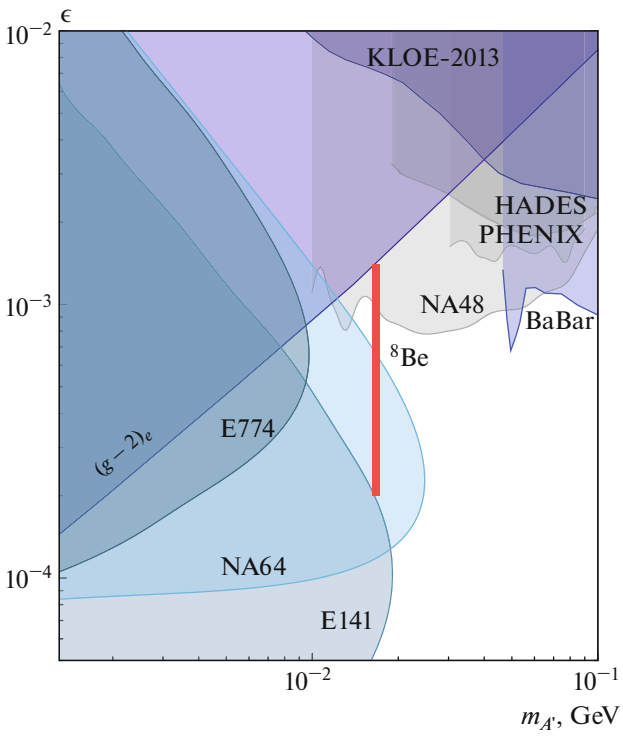

Fig. 7. The 90% C.L. exclusion area in the $(m_\chi; \epsilon)$ from the NA64 experiment (blue area). For the mass of 16.7 MeV, the $X - e$ coupling region excluded by NA64 is $1.2 \times 10^{-4} < \varepsilon_e < 6.8 \times 10^{-4}$.

5.1.3. Visible mode. The ^{8}Be anomaly. The ATOMKI experiment of Krasznahorkay et al. [26] has reported the observation of a 6.8σ excess of events in the invariant mass distributions of e^+e^- pairs produced in the nuclear transitions of excited ^{8}Be* to its ground state via internal pair creation. This anomaly can be interpreted as the emission of a new protophobic gauge X boson with a mass of 16.7 MeV followed by its $X \to e^+e^-$ decay assuming that the X has non-universal couplings to quarks, coupling to electrons in the range $2 \times 10^{-4} \lesssim \epsilon_e \lesssim 1.4 \times 10^{-3}$ and the lifetime $10^{-14} \lesssim \tau_X \lesssim 10^{-12}$ s [54]. It has motivated worldwide theoretical and experimental efforts towards light and weakly coupled vector bosons, see, e.g. [93–99]. Another strong motivation to the search for a new light boson decaying into e^+e^- pair is provided by the Dark Matter puzzle discussed previously.

The NA64e combined 90% C.L. exclusion limits on the mixing ε as a function of the A' mass are shown in Fig. 7 together with the current constraints from other experiments [100]. The NA64 results exclude the X-boson as an explanation of the ^{8}Be* anomaly for the

$X - e^-$ coupling $\epsilon_e \lesssim 6.8\times10^{-4}$ and the mass value of 16.7 MeV, leaving the still unexplored region $6.8\times10^{-4} \lesssim \epsilon_e \lesssim 1.4\times10^{-3}$ for further searches. Note that in recent paper [101] the last NA64 data [100] has been analyzed. It was shown that at 90% C.L. models with pure vector or axial vector couplings of electron with $X(16.7)$ boson are excluded but the chiral couplings $V \pm A$ are still possible and moreover it is possible to explain both electron $g_e - 2$ and muon $g_\mu - 2$ anomalies [101].

Very recently the ATOMKI group reported a similar excess of events at approximately the same invariant mass in the nuclear transitions of another nucleus, ^{4}He [102]. This dramatically increases the importance of confirmation of the observed excess by another nuclear physics experiment, as well as independent searches for the X in a particle physics experiment. Therefore, the NA64 experimental approach based on the using two independent electromagnetic calorimeters, one as an activedump (WCAL) for the X boson production and another one (ECAL) for the $X \to e^+e^-$ decay detection is extremely timely. To cover the remaining parameter space for the $X - e$ couplings, which corresponds to a very short-lived X boson case with a lifetime $\tau_X \lesssim 10^{-13}$ s, is very challenging. A more accurate future measurement after LS2 should include also the e^+e^- pair invariant mass reconstruction. This requires the use of a high-precision tracker with an excellent two-track resolution capability combined with a magnetic spectrometer for the accurate decay electron and positron momenta measurements to finally reconstruct the invariant mass of the X with a good precision. For this NA64e will need a substantial upgrade of the current setup with a new high-resolution trackers, e.g. based on micromegas detectors, a new WCAL with a better optimised thickness, and a new synchrotron radiation detector with higher granularity. This makes further searching quite challenging but very exciting and important.

5.1.4. NA64*e* and the search for *Z'* boson coupled with $L_\mu - L_\tau$ current. Light Z' boson which couples with $L_\mu - L_\tau$ current will mix with ordinary photon at one-loop level [28]. Namely, an account of one-loop propagator diagrams with virtual μ- and τ-leptons leads to nonzero $\gamma - Z'$ kinetic mixing $-\frac{\epsilon}{2}F^{\mu\nu}Z'_{\mu\nu}$ where ϵ is the finite mixing strength given by [13]

$$\epsilon_{1l} = \frac{8}{3}\frac{ee_\mu}{16\pi^2}\ln\left(\frac{m_\tau}{m_\mu}\right) = 1.4\times10^{-2}\times e_\mu. \qquad (54)$$

Here e is the electron charge, e_μ is electron Z' charge and m_μ, m_τ are the muon and tau lepton masses respectively. It should be stressed that we assume that possible tree level mixing $-\frac{\epsilon_{\text{tree}}}{2}F^{\mu\nu}Z'_{\mu\nu}$ is absent or much smaller than one-loop mixing $\frac{\epsilon_{1l}}{2}F^{\mu\nu}Z^{\mu\nu}$. To be precise, we assume that there is no essential cancellation between tree-level and one-loop mixing terms $\left|\epsilon_{\text{tree}} + \epsilon_{1l}\right| \geq \left|\epsilon_{1l}\right|$. For $m_{Z'} \ll m_\mu$ the value $e_\mu = (4.8 \pm 0.8)\times10^{-4}$ from Eq.(54) leads to the prediction of the corresponding mixing value

$$\epsilon_{1l} = (6.7 \pm 1.1)\times10^{-6}. \qquad (55)$$

Thus, one can see that the Z' interaction with the $L_\mu - L_\tau$ current induces at one-loop level the $\gamma - Z'$ mixing of Z' with ordinary photon which allows to probe Z' not only in muon or tau induced reactions but also with intense electron beams. In particular, this loophole opens up the possibility of searching the new weak leptonic force mediated by the Z' in experiments looking for dark photons (A'). The fact that the $\gamma - Z'$ mixing of Eq. (55) is at an experimentally interesting level is very exciting. We point out further that a new intriguing possibilities for the complementary searches of the Z' in the currently ongoing experiment NA64 [31, 34] exists. Indeed, the NA64 aimed at the direct search for invisible decay of sub-GeV dark photons in the reaction $e^- + Z \to e^- + Z + A'$; $A' \to$ invisible of high energy electron scattering off heavy nuclei [31]. The experimental signature of the invisible decay of Z' produced in the reaction $e^- + Z \to e^- + Z + Z'$; $Z' \to$ invisible due to mixing of Eq. (54) is the same—it is an event with a large missing energy carried away by the Z'. Thus, by using Eq. (55) and bounds on the $\gamma - A'$ mixing the NA64 can also set constraints on coupling e_μ.

The current NA64 bounds on the ϵ parameter for the dark photon mass region $1 \lesssim m_{Z'} \lesssim 10$ MeV are in the range $0.7\times10^{-5} \lesssim \epsilon \lesssim 3\times10^{-5}$ [34]. Taking into account that the sensitivity of the experiment scales as $\epsilon \sim 1/\sqrt{n_{\text{EOT}}}$, results in required increase of statistics by a factor $\simeq 30$ in order to improve sensitivity up to the mixing value of Eq. (55) for this Z' mass region. This would allow either to discover the Z' or exclude it as an explanation of the $g_\mu - 2$ anomaly for the substantial part of the mass range $m_{Z'} \ll m_\mu$ by using the electron beam. The direct search for the Z' in missing-energy events in the reaction $\mu Z \to \mu ZZ'$; $Z' \to$ invisible in the dedicated experiment with the muon beam at CERN would then be an important cross check of results obtained with the electron beam. Let us note that the mixing given by the Eq. (55) would also lead

to an extra contribution to the elastic $\nu e \to \nu e$ scattering signal in the solar neutrino measurement at the Borexino experiment [103]. The BOREXINO data on the elastic $\nu_\mu e$ scattering [104] lead to lower bound on $m_{Z'} \geq (5\text{–}10)$ MeV by assuming that muon anomaly is explained due to existence of light Z' boson interacting with $L_\mu - L_\tau$ current and there is no tree level mixing between photon and Z', i.e. $\epsilon_{\text{tree}} = 0$. The measurement of $\nu - e$ elastic scattering in the LSND experiment [68] set a similar bound to the e_μ coupling for $m_{Z'} \lesssim 10$ MeV [103]. The expected 90% C.L. NA64 exclusion regions in the $(m_{Z'}, e_\mu)$ plane (dashed curves) from the measurements with the electron beam for $\simeq 4\times10^{12}$ and $\simeq 4\times10^{13}$ EOT and muon beams for $\simeq 10^{12}$ muons on target (MOT) [28] are shown in Fig. 8. Constraints from the BOREXINO [103], CCFR [105], and BABAR [62] experiments, as well as the BBN excluded area [103, 106] are also shown. The parameter space shown in Fig.8 could also be probed by other electron experiments such as Belle II [107], BDX [108, 109], and LDMX [110], which would provide important complementary results.

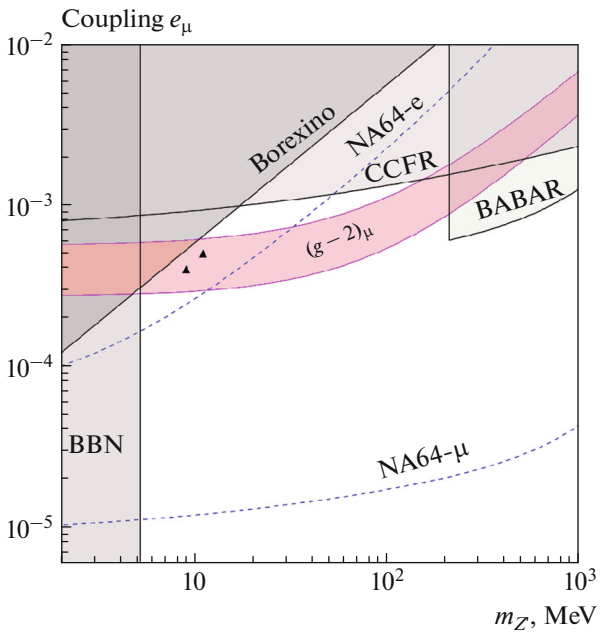

Fig. 8. The NA64 90% C.L. expected exclusion regions in the $(m_{Z'}, e_\mu)$ plane (dashed curves) from the measurements with the electron (NA64e, $\simeq 4\times10^{12}$ EOT) and muon (NA64μ, $\simeq 10^{12}$ MOT) beams, taken from ref. [111, 112]. Two triangles indicate reference points corresponding to the mass $m_{Z'} = 9$ and 11 MeV, and coupling $e_\mu = 4\times10^{-4}$ and 5×10^{-4}, respectively, which are used to explain the IceCube results, see ref. [103] for details.

*5.2. The Experiment NA64*μ

Recently, the NA64 collaboration proposed to carry out further searches for dark sector and other rare processes in missing energy events from high energy muon interactions in a hermetic detector at the CERN SPS [111, 112].

A dark sector of particles predominantly weakly-coupled to the second and possibly third generations of the SM is motivated by several theoretically interesting models. Additional to gravity this new very weak interaction between the visible and dark sector could be mediated either by a scalar (S_μ) or $U'(1)$ gauge bosons (Z_μ) interacting with ordinary muons. In a class of $L_\mu - L_\tau$ models the corresponding Z_μ could be light and have the coupling strength lying in the experimentally accessible region. If such Z_μ mediator exists it could also explain the muon $g_\mu - 2$ anomaly—the discrepancy between the predicted and measured values of the muon anomalous magnetic moment [111].

The proposed extension of the NA64 experiment called NA64μ aiming mainly at searching for invisible decays of the Z_μ either to neutrinos or LDM particles [112]. The primary goal of the experiment in the 2021 pilot run with the $\simeq$ 100–160 GeV M2 beam is to commission the NA64μ detector and to probe for the first time the still unexplored area of the coupling strengths and masses $M_{Z_\mu} \lesssim 200$ MeV that could explain the muon $g_\mu - 2$ anomaly. Another strong point of NA64μ is its capability for a sensitive search for dark photon mediator (A') of DM production in invisible decay mode in the mass range $m_{A'} \gtrsim m_\mu$, thus making the experiment extremely complementary to the ongoing NA64e and greatly increases the discovery potential of sub-GeV dark matter. Other searches for S_μ's decaying invisibly to dark sector particles, and millicharged particles will probe a still unexplored parameter areas [112].

5.2.1. Searching for the $\mu + Z \to \mu + Z + Z_\mu$, $Z_\mu \to \nu\bar{\nu}$. The reaction of the Z_μ production is a rare event. For the previously mentioned parameter space, it is expected to occur with the rate $\lesssim \alpha_\mu/\alpha \sim 10^{-6}$ with respect to the ordinary photon production rate. Hence, its observation presents a challenge for the detector design and performance. The experimental setup specifically designed to search for the Z_μ is schematically shown in Fig. 9.

The experiment could employ the upgraded muon beam at the CERN SPS. The beam was designed to transport high fluxes of muons of the maximum momenta in the range between 100 and 225 GeV/c

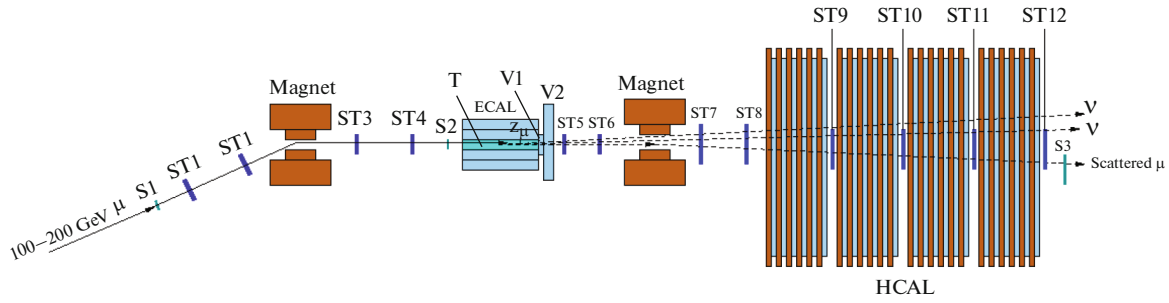

Fig. 9. Schematic illustration of the NA64μ setup to search for invisible Z_μ decays in the reaction $\mu Z \to \mu Z Z_\mu$ [111].

that could be derived from a primary proton beam of 450 GeV/c with the intensity between 10^{12} and 10^{13} protons per SPS spill. The detector shown in Fig. 9 utilizes two, upstream and downstream, magnetic spectrometer sections consisting of dipole magnets and a set of low-material budget straw tubes chambers, ST1–ST4 and ST5–ST6, respectively, allowed reconstruction and precise measurements of incident and scattered in a target muons. It also uses scintillating fiber hodoscopes S1, S2, defining the primary muon beam, and S3, S4, and S5 defining the scattered muons, the active target T surrounded by a high efficiency electromagnetic calorimeter (ECAL) serving as a veto against photons and other secondaries emitted from the target at large angles. Downstream the target the detector is equipped with high efficiency forward veto counters V1 and V2 and a massive, completely hermetic hadronic calorimeter (HCAL) located at the end of the setup to detect energy deposited by secondaries from the $\mu^- A \to$ *anything* primary muon interactions with nuclei A in the target. The HCAL has lateral and longitudinal segmentation, and also serves for the final state muon identification. For searches at low energies, Cherenkov counters to enhance the incoming muon tagging efficiency can be used.

The method of the search is the following. The bremsstrahlung Z_μs are produced in the reaction

$$\mu + Z \to \mu + Z + Z_\mu, \quad Z_\mu \to \nu\bar{\nu}, \tag{56}$$

from the high energy muon scattering off nuclei in the target. The reaction (56) is typically occurred uniformly over the length of the target. The Z_μ is either stable or decaying invisibly if its mass $M_{Z_\mu} \le 2m_\mu$, or, as shown, it could subsequently decay into a $\mu^+\mu^-$ pair if $M_{Z_\mu} > 2m_\mu$. In the former case, the Z_μ penetrates the T, veto V1, V2 and the massive HCAL without interaction. In the later case, it could decays in flight into a $\mu^+\mu^-$ pair, resulting in the di-muon track signature in the detector. The bremsstrahlung Z_μ then either penetrates the rest of the detector without interactions, resulting in zero-energy deposition in the V1, V2 and HCAL , or it could decay in flight into a $\mu^+\mu^-$ pair if its mass is greater than the mass of two muons. A fraction ($f \lesssim 0.3$) of the primary beam energy $E_\mu = fE_0$ is carried away by the scattered muon which is detected by the second magnetic spectrometer arm. For the radiation length $X_0 \lesssim 1$ cm, and the total thickness of the target $\simeq 30$ cm the energy leak from the target into the V1 is negligibly small. The remained part of the primary muon energy $E_2 = (1-f)E_0$ is transmitted through the "HCAL wall" by the Z_μ, or deposited partly in the HCAL via the Z_μ decay in flight $Z_\mu \to \mu^+\mu^-$. At Z_μ energies $E_{Z_\mu} \lesssim 50$ GeV, the opening angle $\Theta_{\mu^+\mu^-} \simeq M_{Z_\mu}/E_{Z_\mu}$ of the decay $\mu^+\mu^-$ pair is big enough to be resolved in two separated tracks in the M1 and M2 so the pairs are mostly detected as a double track event. The HACL is served as a dump to absorb completely the energy of secondary particles produced in the primary pion or kaon interaction in the target. In order to suppress background due to the detection inefficiency, the detector must be longitudinally completely hermetic. To enhance detector hermeticity, the hadronic calorimeter has the total thickness of $\simeq 28\lambda_{\rm int}$ (nuclear interaction lengths) and placed behind the DV.

The signature of the reaction (56) is

- the presence of incoming muon with energy around 150 GeV,
- the presence of scattered muon with energy $\lesssim 80$ GeV,
- no energy deposition in the HCAL,
- no energy deposition in the HCAL EE.

The occurrence of Z_μ produced in $\mu^- Z$ interactions would appear as an excess of events with a single low energy muon accompanied by zero-energy deposition in the detector. The backgrounds for the reaction (56) have been analyzed in ref. [111, 112]. The main backgrounds are due to μ low-energy tail, HCAL nonhermeticity, μ induced photonuclear reactions

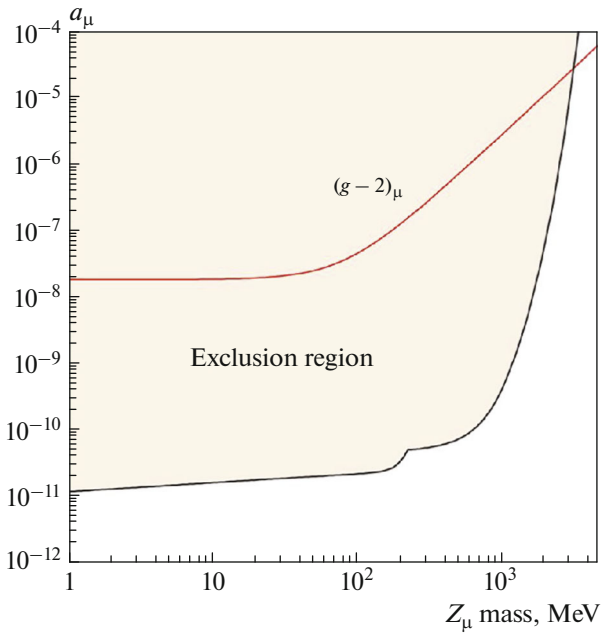

Fig. 10. Expected constraints on the α_μ coupling constant as a function of the Z_μ mass for 10^{12} μ at energy E_μ = 150 GeV [111, 112].

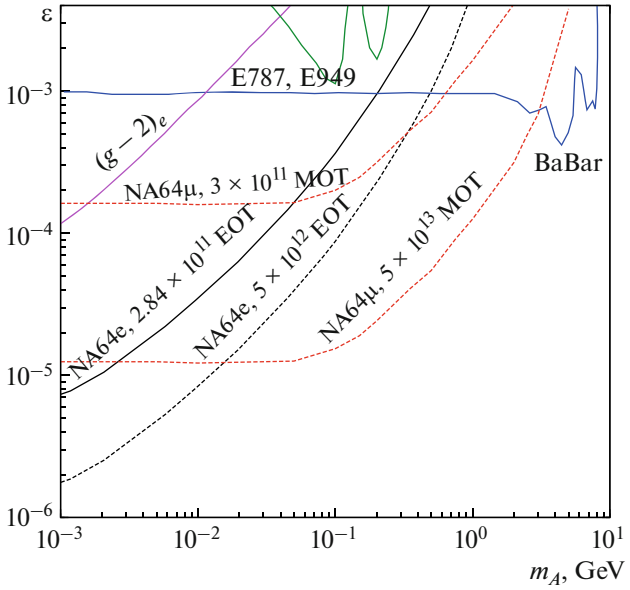

Fig. 11. The NA64e 90% C.L. current [34] and expected exclusion bounds obtained with 2.84×10^{11} EOT and 5×10^{12} EOT, respectively, in the $(m_{A'},\varepsilon)$ plane. The NA64μ projected bounds calculated for $n_{\mathrm{MOT}} = 5\times10^{12}$ and 5×10^{13} are also shown.

and μ trident events [111, 112]. These backgrounds were estimated in ref. [111, 112] and they are rather small $\lesssim 10^{-12}$.

The expected sensitivity of this experiment for α_μ for different Z_μ masses and for 10^{12} muons on target is shown in Fig. 10. Note that in refs. [113–115] the possibility to use muon beam for the search for light scalar particles has been discussed.

In the A' dark photon model muons and electrons interact with the dark photon with the same coupling constant. Hence, similar to the reaction of Eq. (53), the dark photons will be also produced in the reaction of Eq. (56) with the same experimental signature of the missing energy. For the A' mass region $m_{A'} \gg m_e$, the total cross-section of the dark photon electroproduction $eZ \to eZA'$ scales as $\sigma^e_{A'} \sim \epsilon_e^2/m^2_{A'}$. On the other hand, for the dark photon masses, $m_{A'} \lesssim m_\mu$, the similar $\mu Z \to \mu Z A'$ cross-section can be approximated in the bremsstrahlung-like limit as $\sigma^\mu_{A'} \sim \epsilon_\mu^2/m_\mu^2$. Let us now compare expected sensitivities of the A' searches with NA64e and NA64μ experiments for the same number $\simeq 5\times10^{12}$ particles on target. Assuming the same signal efficiency the number of A' produced by the 100 GeV electron and muon beam can approximated, respectively, as follows

$$N^e_{A'} \approx \frac{\rho N_{\mathrm{av}}}{A}\times n_{\mathrm{EOT}} L^e \sigma^e_{A'},$$
$$N^\mu_{A'} \approx \frac{\rho N_{\mathrm{av}}}{A}\times n_{\mathrm{MOT}} L^\mu \sigma^\mu_{A'}, \quad (57)$$

where $L^e \simeq X_0$ and $L^\mu \simeq 40X_0$ are the typical distances that are passed by an electron and muon, respectively, before producing the A' with the energy $E_{A'} \gtrsim 50$ GeV in the NA64 active Pb target of the total thickness of $\simeq 40$ radiation length (X_0) [111]. The detailed comparison of the calculated A' sensitivities of NA64e and NA64μ is shown in Fig. 11, where the 90% C.L. limits on the mixing ε are shown for a different number of particles on target for both the NA64e and NA64μ experiments. The limits were obtained for the background free case by using exact-tree-level (ETL) cross-sections rather than the improved Weizsacker-Williams (IWW) ones calculated for NA64e in ref. [41], and for the NA64μ case in this work. The later are shown in Fig. 12 as a function of $E_{A'}/E_\mu$ for the Pb target and mixing value $\epsilon = 1$. One can see that in a wide range of masses, 20 MeV $\lesssim m_{A'} \lesssim 1$ GeV, the total IWW cross-sections are larger by a factor $\simeq 2$

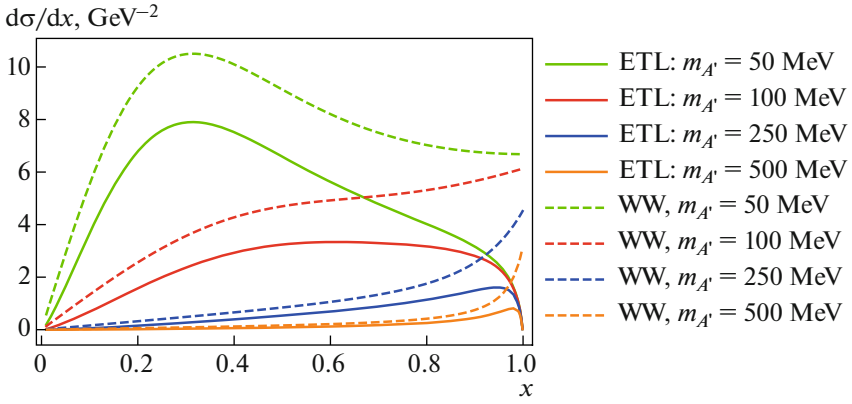

Fig. 12. Cross-section of dark photon production by muons as a function of $x = E_{A'}/E_{\mu}$ for various masses $m_{A'}$, and $\epsilon = 1$. Solid lines represent ETL cross-sections and dashed lines show the cross-sections calculated in IWW approach.

compared to the ETL ones. As the result, the typical limits on ϵ for the ETL case are worse by about a factor $\simeq 1.4$ compared to the IWW case. For $n_{\text{EOT}} = n_{\text{MOT}} = 5\times10^{12}$ the sensitivity of NA64e is enhanced for the mass range $m_e \ll m_{A'} \simeq 100$ MeV while for the A' masses $m_{A'} \gtrsim 100$ MeV NA64μ allows to obtain more stringent limits on ϵ in comparison with NA64e.

5.3. Combined LDM Sensitivity of NA64e and NA64μ [91]

The estimated NA64e and NA64μ limits on the $\gamma - A'$ mixing strength, allow us to set the combined NA64e and NA64μ constraints on the LDM models, which are shown in the $(y; m_\chi)$ plane in Fig. 13. As discussed in Appendix **A**, as a result of the $\gamma - A'$ mixing the cross-section of the DM particles annihilation into the SM particles is proportional to ϵ^2. Hence using constraints on the DM annihilation cross-section one can derive constraints in the $(y \equiv \epsilon^2\alpha_D(m_\chi/m_{A'})^4; m_\chi)$ plane and restrict the LDM models with the masses $m_\chi \lesssim 1$ GeV.

The combined limits [34] obtained from the data sample of the 2016, 2017 and 2018 runs and expected from the run after the LS2 are shown in the top panels of Fig. 13 together with combined limits from NA64e and NA64μ for 10^{13} EOT and 2×10^{13} MOT, respectively. The plots show also the comparison of our results with the limits of other experiments. It should be noted that the χ-yield in the NA64 case scales as ϵ^2 rather than $\epsilon^4\alpha_D$ as in beam dump experiments. Therefore, for sufficiently small values of α_D the NA64 limits will be much stronger. This is illustrated in the upper right panel of Fig. 13, where the NA64 limits are shown for $\alpha_D = 0.1$. One can see that for this or smaller values of α_D the direct search for LDM at NA64e with 5×10^{12} EOT excludes the scalar and Majorana models of the LDM production via vector mediator with $\frac{m_{A'}}{m_\chi} = 3$ for the full mass region up to $m_\chi \lesssim 0.2$ GeV. While being combined with the NA64μ limit, the NA64 will exclude the models with $\alpha_D \leq 0.1$ for the entire mass region up to $m_\chi \lesssim 1$ GeV. So we see that for the full mass range $m_\chi \lesssim 1$ GeV the obtained combined NA64e and NA64μ bounds are more stringent than the limits obtained from the results of NA64e that allows probing the full sub-GeV DM parameter space.

6. OTHER FUTURE EXPERIMENTS

There are a lot of planned experiments devoted to the search for both visible and invisible A' decay modes. Here we briefly describe the most interesting future experiments.

6.1. SHiP at CERN

The proposed experiment SHiP [116] at CERN is intended to look for visible decays $A' \to e^+e^-, \mu^+\mu^-, \pi^+\pi^-$ of long lived A' boson. Also SHiP can search for LDM by detection of the LDM scattering in neutrino detector at the 400 GeV SPS beam line at CERN. The detector consists of OPERA-like bricks of lead and emulsions placed in magnetic field. The LDM detection occurs via electon LDM elastic scattering. The dominant backgrounds are expected related with neutrino scattering processes and can be reduced using

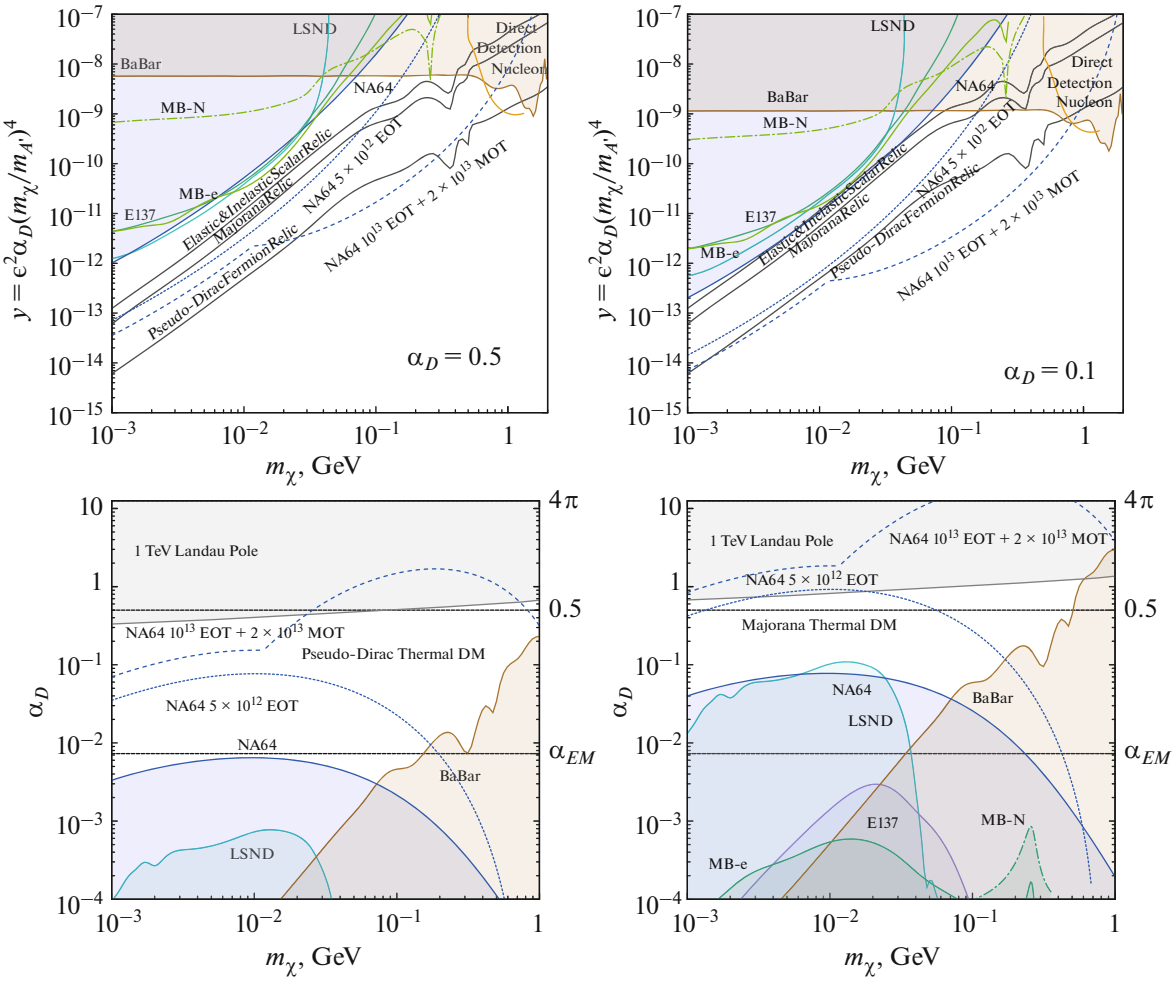

Fig. 13. The NA64 90% C.L. current (solid) [34] and expected (dotted light blue) exclusion bounds for 5×10^{12} EOT in the (m_χ, y) and (m_χ, α_D) planes. The combined limits from NA64e and NA64μ are also shown for 10^{13} EOT plus 2×10^{13} MOT (dashed blue). The limits are calculated for $\alpha_D = 0.1$ and 0.5, and $m_{A'} = 3m_\chi$. The results are also shown in comparison with bounds obtained from the results of the LSND [68], E137 [63], BaBar [62] and MiniBooNE [69] experiments.

several cuts. For $N = 10^{20}$ POT[10] the sensitivity is $y \equiv \epsilon^2\alpha_D\left(\frac{m_\chi}{m_{A'}}\right)^4 \geq 10^{-12}$ for $m_\chi \leq O(1)$ GeV [4].

6.2. Belle-II at KEK

Belle-II [117] is a multi-purpose detector with sensitivity to invisible A' decays via mono-photon in the range $M_{A'} \leq 9.5$ GeV can look for A' invisible decays using the reaction $e^+e^- \to \gamma(A' \to \text{invisible})$. Belle-II also can search for visible A' decays. First data with full luminosity $L_t = 50$ ab^{-1} are expected in 2025. The future sensitivity is $\epsilon^2 \geq 10^{-9}$ for $m_{A'} < 9.5$ GeV.

6.3. MAGIX at MESA

Visible dark photon decay searches with dipole spectrometer MAGIX at the 105 MeV polarized electron beam are planned at MESA accelerator complex [118]. The electroproduction reaction $eZ \to eZA'$ and visible decay mode $A' \to e^+e^-$ will be used to identify the A' as di-electron resonance. The expected sensitivity to the ϵ^2 parameter is up to 10^{-9} for 10 MeV $< m_{A'} <$ 60 MeV.

6.4. PADME at LNF

The reaction $e^+e^- \to \gamma(A' \to \textit{invisible})$ is used for the search for dark photon. For 10^{13} positron on target

[10] POT ≡ protons on target.

the expected sensitivity is $\epsilon^2 \geq 10^{-7}$ for $m_{A'} < 24$ MeV [119]. The collection of data started at the end of 2018.

6.5. VEPP3 at BINP

The proposed experiment at BINP [120] is similar to PADME experiment. The expected sensitivity is planned to be $\epsilon^2 \geq 10^{-8}$ in the range $5 < m_{A'} < 22$ MeV.

6.6. BDX at JLab

BDX ar JLab is an electron beam-dump experiment [108, 109]. The experiment is sensitive to elastic DM scattering $e\chi \to e\chi$ in the far detector after electron nuclei production in $eZ \to eZ(A' \to \chi\bar{\chi})$. The expected sensitivity is $y \geq 10^{-13}$ for $1 \text{ MeV} < m_\chi < 100$ MeV.

6.7. DarkLight at JLab

In this experiment dark photons are produced in the reaction $ep \to epA'$ colliding the 100 MeV electron beam on a gaseous hydrogen target [121, 109]. The main peculiarity of this experiment is the possibility to detect the scattered electron and recoil proton, enabling the reconstruction of invisible A' decays. Also the search for visible $A' \to e^+e^-$ decays is possible. The expected sensitivity is $\epsilon^2 \geq 10^{-6}$ for $10 \text{ MeV} < m_{A'} < 80$ MeV.

6.8. LDMX

This experiment is similar to NA64 experiment and will use the electroproduction reaction $eZ \to eZ(A' \to \chi\bar{\chi})$ for the dark photon search [110]. The LDMX(Light Dark Matter Experiment) will measure both missing energy and missing momentum that is extremely important for background suppression. The expected sensitivity for the ε parameter is up to 10^{-6} for $m_{A'} = 1$ MeV [110]. The extended LDMX will be able to increase sensitivity to the ϵ parameter by factor 10.

7. CONCLUSIONS

Active beam-dump searches for dark sector physics in missing energy events have been proven by the NA64 experiment to be very powerful and sensitive via both invisible and visible decays of dark vector mediator. The future combined sensitivity of searches with both electron and muon beams has a great potential to probe a large region of the remaining LDM parameter space, especially towards the higher LDM masses. Remarkably, that with the statistics accumulated during years 2016–2018 NA64 already starts probing the sub-GeV DM parameter space. While with 5×10^{12} EOT NA64 with electron beam is able to test the scalar and Majorana LDM scenarios for $\frac{m_{A'}}{m_\chi} \geq 2.5$. The combined NA64 results with electron and muon beams and with 10^{13} EOT, 2×10^{13} MOT, respectively, will allow to fully explore the parameter space of other interesting LDM models like pseudo-Dirac DM model or the model with new light vector boson Z_μ. This makes NA64e and NA64μ extremely complementary to each other, as well as to the planned LDMX experiment [110], and greatly increases the NA64 discovery potential of sub-GeV DM.

There are several alternatives [7] to the dark photon model based on the use of gauge symmetries like $U(1)_{B-L}$ or $U(1)_{B-3e}$. As in the dark photon model the observed value of the LDM density allows to estimate the coupling constant ϵ of new light Z' boson with electron. The value of the ε parameter for such models coincides with the ε value for dark photon model up to some factor $k \leq 3$ [7], so NA64e can also test such models. For instance, for the model with $(B-L)$ vector interaction NA64e is able to exclude scalar and Majorana LDM scenarios in full analogy with the case of dark photon model.

However it should be stressed that for $m_{A'} \approx 2m_\chi$ the DM annihilation cross-section is proportional to $(m_{A'}^2 - 4m_\chi^2)^{-2}$. As a consequence the predicted value of the ϵ^2 parameter is proportional to $\left(\frac{m_{A'}^2}{4m_\chi^2} - 1\right)^2$ that can reduce the ϵ^2 value by (2–4) orders of magnitude in comparison with the reference point $\frac{m_{A'}}{m_\chi} = 3$ [92]. It means that NA64 experiment as other future experiments like LDMX [110] are not able to test the region $m_{A'} \approx 2m_\chi$ completely[11].

Current accelerator experimental data[12] restrict rather strongly the explanation of the $g_\mu - 2$ muon anomaly due to existence of new light gauge boson but not completely eliminate it. The most popular model where dark photon A' interacts with the SM electro-

[11] The values of $m_{A'}$ and m_χ are arbitrary, so the case $m_{A'} \approx 2m_\chi$ could be considered as some fine-tuning. It is natural to assume the absence of significant fine-tuning. In this paper we require that $\left|\frac{m_{A'}}{2m_\chi} - 1\right| \geq 0.25$.

[12] The review of nonaccelerator bounds can be found in ref. [83].

magnetic current due to mixing $\frac{\epsilon}{2}F_{\mu\nu}F'^{\mu\nu}$ term is excluded. The Borexino data on neutrino electron elastic scattering exclude the models where Z' interacts with both leptonic and $B-L$ currents. The interaction of the Z' boson with $L_\mu - L_\tau$ current is excluded for $m_{Z'} \geq 214$ MeV while still leaving the region of lower masses unconstrained. NA64μ is able to test the model with $L_\mu - L_\tau$ interaction at $m_{Z'} \leq 214$ MeV as a model explaining muon $g_\mu - 2$ anomaly.

APPENDIX A: DM Density Calculations

The observed homogeneity and isotropy of the Universe enable us to describe the overall geometry and evolution of the Universe in terms of two cosmological parameters accounting for the spatial curvature and the overall expansion (or contraction) of the Universe that is realized in the Freedman–Robertson–Walker metric[13]

$$ds^2 = dt^2 - R^2(t)\left[\frac{dr^2}{1-kr^2} + r^2(d\theta^2 + \sin^2\theta d\Phi^2)\right]. \quad (58)$$

The curvature constant k takes three values $k = 1, -1, 0$ that corresponds to closed, open and spationally flat geometries. The cosmological equations are derived from Einstein's equations

$$R_{\mu\nu} - \frac{1}{2}g_{\mu\nu} = 8\pi G_N T_{\mu\nu} + \Lambda g_{\mu\nu}. \quad (59)$$

We shall use the standard assumption that an effective energy-momentum tensor $T_{\mu\nu}$ is a perfect fluid, for which

$$T\mu\nu = -pg_{\mu\nu} + (p+\rho)u_\mu u_\nu, \quad (60)$$

where p is the pressure, ρ is the energy-density and $u = (1,0,0,0)$ is the velocity vector for the isotropic fluid in co-moving coordinates. For the metric (58) and the energy-momentum tensor (60) the Einstein equations (59) lead to Friedman–Lemaitre equations

$$H^2 = \frac{8\pi G_N \rho}{3} - \frac{k}{R^2} + \frac{\Lambda}{3}, \quad (61)$$

$$\frac{1}{a^2(t)}\frac{d^2a}{dt^2} = \frac{\Lambda}{3} - \frac{4\pi G_N}{3}(\rho + 3p), \quad (62)$$

$$H(t) \equiv \frac{1}{R(t)}\frac{dR}{dt}, \quad (63)$$

where $H(t)$ is the Hubble parameter and Λ is cosmological constant. Energy conservation $T^{\mu\nu}_{;\nu} = 0$ leads to the equation

$$\frac{d\rho}{dt} = -3H(\rho + p). \quad (64)$$

The equation (64) allows to determine today critical density ρ_c that corresponds to flat Universe with $k = 0$ and $\Lambda = 0$ in the equations (61), (62), namely

$$\rho_c = \frac{3H^2}{8\pi G_N} = 1.05\times10^{-5}h^2 \text{ GeV cm}^{-3} \quad (65)$$

Here the parameter h is defined by

$$H \equiv 100 \text{ h km s}^{-1} \text{ Mpc}^{-1} \quad (66)$$

and its experimental value is $h = 0.72 \pm 0.03$ [9]. The cosmological density parameter Ω_{tot} is defined as the energy density relative to the critical density

$$\Omega_{\text{tot}} = \rho/\rho_c. \quad (67)$$

One can rewrite the equation (61) in the form

$$\frac{k}{R^2} = H^2(\Omega_{\text{tot}} - 1). \quad (68)$$

As a consequence of the equation (68) we see that for $\Omega_{\text{tot}} > 1$ the Universe is closed, for $\Omega_{\text{tot}} < 1$ the Universe is open and for $\Omega_{\text{tot}} = 1$ the Universe is spatially flat. It is often necessary to distinguish different contributions to the density Ω_{tot}. It is convenient to define present-day density parameters for pressureless matter Ω_m and relativistic particles Ω_r plus the vacuum dark energy density Ω_V and the dark matter density Ω_d. Current data give [9]

$$\Omega_V = 0.73 \pm 0.01, \quad (69)$$

$$\Omega_d = 0.23 \pm 0.01. \quad (70)$$

It is expected that the early Universe can be described by a radiation-dominated equation of state. In addition it is assumed that through much of the radiation-dominated period, thermal equillibrium is established by the rapid rate of particle interactions relative to the expansion rate of the Universe. In equilibrium thermodynamic quantities like energy density, pressure and entropy are calculable quantities in the ideal gas approximation. The density of states for particle i is given by

$$dn_i = \frac{g_i d^3\vec{p}}{(2\pi)^3}\left(\exp\left[\frac{E_i - \mu_i}{T_i}\right] \pm 1\right)^{-1}. \quad (71)$$

Here g_i counts the number of degrees of freedom of particle i, $E_i^2 = \vec{p}^2 + m_i^2$, $\pm$ corresponds to either

[13] As a review, see for example [1, 2].

Fermi or Bose statistics, μ_i is the chemical potential[14] and T_i is the temperature. The energy density, the pressure, the number density and the entropy density are given by the formulae

$$\rho_i = \int E_i dn_i, \tag{72}$$

$$p_i = \frac{1}{3}\int \frac{\vec{p}_i^{\,2}}{E_i} dn_i, \tag{73}$$

$$n_i = \int dn_i, \tag{74}$$

$$s_i = \frac{\rho_i + p_i - \mu_i n_i}{T_i}. \tag{75}$$

For instance, for photons with $g_\gamma = 2$ polarization states the energy density, pressure, density of the number of photons and the entropy density are given by the formulae

$$\rho_\gamma = \frac{\pi^2}{15} T^4, \tag{76}$$

$$p_\gamma = \frac{1}{3}\rho_\gamma, \tag{77}$$

$$s_\gamma = \frac{4\rho_\gamma}{3T}, \tag{78}$$

$$n_\gamma = 0.243 T^3. \tag{79}$$

The number density of nonrelativistic particles is given by the formula

$$n_{\text{nonrel}} = g\frac{1}{(2\pi)^{3/2}}(mT)^{3/2}\exp\left(-\frac{m}{T}\right), \tag{80}$$

where g is the number of polarizations. As a consequence of the equations (61), (62) and the definition (75) of the entropy density one can find that the total entropy is conserved, namely

$$\frac{d(sR^3)}{dt} = 0. \tag{81}$$

At the very high temperatures associated with the early Universe, massive particles are pair produced, and are part of the thermal bath. At high temperature $T \gg m_i$ we can neglect masses and approximate the energy density by including those particles with $m_i \ll T$, namely

$$\rho = \left(\sum_B g_B + \frac{7}{8}\sum_F g_F\right)\frac{\pi^2}{30} T^4 \equiv g_\rho T^4, \tag{82}$$

where $g_{B(F)}$ is the number of degrees of freedom of each boson (fermion) and the sum runs over all bosons and fermions with $m \ll T$. The factor $7/8$ is due to the difference between the Fermi and Bose integrals (71)–(75). The equation (82) defines the effective number of degrees of freedom. For instance, for temperature $m_e < T < m_\mu$ the effective number $g_\rho = 43/4$.

To obtain estimate of dark matter density we have to solve the Boltzmann equation

$$\frac{dn_d}{dt} + 3H(T)n_d = -\langle\sigma v_{\text{rel}}\rangle(n_d^2 - n_{d,\text{eq}}^2). \tag{83}$$

Here

$$n_d(T) = \int \frac{d^3p}{2\pi^3} f_d(p,T), \tag{84}$$

and $f_d(p,T)$ is DM distribution function. The equilibrium nonrelativistic DM density is

$$n_{d,\text{eq}} = g_d\frac{1}{(2\pi)^{3/2}}(m_\chi T)^{3/2}\exp\left(-\frac{m_\chi}{T}\right), \tag{85}$$

where m_χ is the mass of DM particle. The $\langle\sigma v\rangle$ is thermally pair averaged cross section [1, 122]

$$\langle\sigma v\rangle = \frac{1}{8m_\chi^4 T K_2\left(\frac{m_\chi}{T}\right)^2} \times \int_{4m_\chi^2}^{\infty} ds\sigma(s)\sqrt{s}(s - 4m_\chi^2)K_1\left(\frac{\sqrt{s}}{T}\right). \tag{86}$$

In nonrelativistic approximation $\left\langle\frac{m_\chi \vec{v}^{\,2}}{2}\right\rangle = \frac{3T}{2}$.

The DM relative density parameter Ω_d is represented in the form

$$\Omega_d = \frac{m_\chi s_o Y_0}{\rho_c}, \tag{87}$$

where $s_0 \equiv s(T_0)$ is today dark entropy density and $Y \equiv \frac{n_d}{s}$ is approximately constant for iso-entropic Universe ($Y(t_d) \approx Y(t_0)$). The evolution equation for $Y(t)$ reads

$$\frac{dY}{dt} = -s\langle\sigma_{\text{rel}}\rangle(Y^2 - Y_{\text{eq}}^2). \tag{88}$$

The equation (88) can be rewritten in the form

$$\frac{dY}{dx} = \frac{1}{3H}\frac{ds}{dx}\langle\sigma_{\text{rel}}\rangle(Y^2 - Y_{\text{eq}}^2). \tag{89}$$

Here $x = \frac{m_\chi}{T}$ and T is photon temperature. Note that for the flat Universe the Hubble parameter $H = \left(\frac{8}{3}\pi G\rho\right)^{1/2}$. The effective degrees of freedom for the energy and entropy densities are defined by

$$\rho = g_{\text{eff}}(T)\frac{\pi^2}{30} T^4, \tag{90}$$

$$s = h_{\text{eff}}(T)\frac{2\pi^2}{45} T^3 \tag{91}$$

[14] For the Universe the effects of nonzero chemical potential are small so we shall use the approximation with zero chemical potentials $\mu_i = 0$.

respectively, in such a way that the $g_{\rm eff}(T) = h_{\rm eff}(T) = 1$ for a relativistic species with one internal or spin degree of freedom. Taking into account (91) equation (89) takes the form

$$\frac{dY}{dx} = -\left(\frac{45}{\pi}G\right)^{-1/2}\frac{g_*^{1/2}m_\chi}{x^2}\langle\sigma v_{\rm rel}\rangle(Y^2 - Y_{\rm eq}^2), \qquad (92)$$

where

$$g_*^{1/2} = \frac{h_{\rm eff}}{g_{\rm eff}^{1/2}}\left(1 + \frac{1}{3}\frac{T}{h_{\rm eff}}\frac{dh_{\rm eff}}{dT}\right). \qquad (93)$$

The equilibrium density $Y_{\rm eq}$ is given by

$$Y_{\rm eq} = \frac{45g}{4\pi^2}\frac{x^2K_2(x)}{h_{\rm eff}\left(\frac{m_\chi}{x}\right)}. \qquad (94)$$

The solution of the equation (92) allows to determine the freeze-out temperature T_d. The decoupling temperature T_d is usually defined by the equation

$$\Delta \equiv Y - Y_{\rm eq} = \delta Y_{\rm eq}. \qquad (95)$$

In the approximation $\frac{d\Delta}{dx} = 0$ the equation

$$\left(\frac{45}{\pi}G\right)^{-1/2}\frac{g_*^{1/2}m_\chi}{x^2}\langle\sigma v_{\rm rel}\rangle Y_{\rm eq}\delta(\delta+2) = -\frac{d\ln Y_{\rm eq}}{dx} \qquad (96)$$

allows to determine the decoupling temperature T_d. The parameter δ is usually taken to be $\delta = 1.5$. After the decoupling we can neglect $Y_{\rm eq}$ in the equation (83) and the integration from T_d to T_0 gives [1, 122]

$$\frac{1}{Y_0} = \frac{1}{Y_d} + \left(\sqrt{\frac{\pi}{45}}M_{\rm PL}\right)^{-1}\left[\int_{T_0}^{T_d}(g_*^{1/2}(\langle\sigma v\rangle)dT\right]. \qquad (97)$$

Numerically $Y_d \gg Y_o$ and we can neglect it, so we obtain [1, 122]

$$Y_o \approx \sqrt{\frac{\pi}{45}}M_{\rm PL}\left[\int_{T_0}^{T_{\rm dec}}(g_*^{1/2}(\langle\sigma v\rangle)dT\right]^{-1}. \qquad (98)$$

The DM relic density can be numerically estimated as

$$\Omega_d h^2 = 8.76\times10^{-11}\ {\rm GeV}^{-2}\left[\int_{T_0}^{T_d}(g_*^{1/2}\langle\sigma v\rangle)\frac{dT}{m_\chi}\right]^{-1}. \qquad (99)$$

In nonrelativistic approximation with $\langle\sigma v_{\rm rel}\rangle = \sigma_o x_f^{-n}$ one can find that the previous formula takes the form [1, 122][15]

$$\Omega_{\rm DM}h^2 = 0.1\left(\frac{(n+1)x_f^{n+1}}{(g_{*s}/g_*^{1/2})}\right)\frac{0.876\times10^{-9}\ {\rm GeV}^{-2}}{\sigma_0}, \qquad (100)$$

where $x_f = \frac{m_\chi}{T_d}$. The following approximate formula [1] takes place for x_f:

$$x_f = c - \left(n + \frac{1}{2}\right)\ln(c), \qquad (101)$$

$$c = \ln(0.038(n+1)\frac{g}{\sqrt{g_*}}M_{\rm Pl}m_\chi\sigma_0). \qquad (102)$$

Here g_*, g_{*s} are the effective relativistic energy and entropy degrees of freedom and g is an internal number of freedom degree. If DM particles differ from DM antiparticles $\sigma_o = \frac{\sigma_{an}}{2}$.

For s-wave annihilation cross-section with $n = 0$

$$\langle\sigma v_{\rm rel}\rangle = 7.3\times10^{-10}\ {\rm GeV}^{-2}\times\frac{1}{g_{*,\rm av}^{1/2}}\left(\frac{m_\chi}{T_d}\right). \qquad (103)$$

Here $g_{*,\rm av}^{1/2} = \frac{1}{T_d}\int_{T_o}^{T_d}(g_{*s}/g_*^{1/2})dT$. The calculations show that $1 \le c_s \equiv \frac{m_\chi}{10T_d} \le 1.5$ at 1 MeV $\le m_\chi \le$ 100 MeV. So we find that

$$\langle\sigma v_{\rm rel}\rangle = 7.3\times10^{-9}\ {\rm GeV}^{-2}\times\frac{1}{g_{*,\rm av}^{1/2}}c_S. \qquad (104)$$

For the Dirac fermion DM χ with dark photon as a messenger between DM and SM sectors the nonrelativistic annihilation cross-section into electron positron pair is[16]

$$\sigma_{an}(\chi\overline{\chi}\to e^-e^+)v_{\rm rel} = \frac{16\pi\varepsilon^2\alpha_{\rm D}m_\chi^2}{(m_{A'}^2 - 4m_\chi^2)^2}. \qquad (105)$$

$$\epsilon^2\alpha_{\rm D} = 2.0\times10^{-8}\ {\rm GeV}^{-2}\times\frac{(m_{A'}^2 - 4m_\chi^2)^2}{m_\chi^2}\frac{2c_s}{g_{*,\rm av}^{1/2}}. \qquad (106)$$

For $m_{A'} = 3m_\chi$ we find

$$\epsilon^2\alpha_{\rm D} = 0.5\times10^{-12}\times\left(\frac{m_\chi}{\rm MeV}\right)^2\times\frac{2c_s}{g_{*,\rm av}^{1/2}}. \qquad (107)$$

At 20 MeV $\le m_\chi \le$ 200 MeV and $T \le 100$ MeV the effective value $g_{*,\rm av}^{1/2} \approx 3.3$, so we find that

$$\epsilon^2\alpha_{\rm D} \sim 0.4\times10^{-12}\times\left(\frac{m_\chi}{\rm MeV}\right)^2. \qquad (108)$$

Note that for pseudo-Dirac DM the predicted value for $\epsilon^2\alpha_{\rm D}$ is bigger than the corresponding value for fermion DM. For the p-wave cross-section in non-

[15] Here $n = 0$ corresponds to s-wave annihilation and $n = 1$ corresponds to p-wave annihilation.

[16] Here we assume that $m_\chi \gg m_e$.

relativistic approximation $\langle \sigma v_{\rm rel} \rangle = \langle B v_{\rm rel}^2 \rangle = 6B\left(\frac{T}{m_\chi}\right)$. An analog of the formula (103) is

$$6B = 14.6\times 10^{-10}\ \text{GeV}^{-2} \times \frac{1}{g_{*,\rm av}^{1/2}}\left(\frac{m_\chi}{T_d}\right)^2. \quad (109)$$

Here $g_{*,\rm av}^{1/2} = \frac{2}{T_d^2}\int_{T_o}^{T_d} T(g_{*s}/g_*^{1/2})dT$. For the p-wave annihilations the estimates are similar to the Dirac fermion case, namely for 1 MeV $\le m_\chi \le$ 200 MeV we find that $\frac{m_\chi}{T_d} = 10\times c_p$ with $1 \le c_p \le 2$.

For the charged scalar DM the nonrelativistic annihilation cross-section into electron-positron pair is

$$\sigma v_{\rm rel} = \frac{8\pi}{3}\frac{\epsilon^2\alpha\alpha_{\rm D} m_\chi^2 v_{\rm rel}^2}{(m_{A'}^2 - 4m_\chi^2)^2}, \quad (110)$$

An analog of the formula (106) is

$$\epsilon^2\alpha_{\rm D} = 4.0\times 10^{-7}\ \text{GeV}^{-2}\frac{(m_{A'}^2 - 4m_\chi^2)^2}{m_\chi^2}\frac{2c_p^2}{g_{*,\rm av}^{1/2}}. \quad (111)$$

For $m_{A'} = 3m_\chi$ we find

$$\epsilon^2\alpha_{\rm D} = 10^{-11}\times\left(\frac{m_\chi}{\text{MeV}}\right)^2\frac{2c_p}{g_{*,\rm av}^{1/2}}. \quad (112)$$

As a reasonable estimate we take

$$\epsilon^2\alpha_{\rm D} \sim 10^{-11}\times\left(\frac{m_\chi}{\text{MeV}}\right)^2. \quad (113)$$

For Majorana fermions the typical estimate for $\epsilon^2\alpha_{\rm D}$ has additional factor ≈ 2.

APPENDIX B: Detection of Long Lived Particles at NA64

In pseudo-Dirac scenario [4] the Majorana particles χ_1 and χ_2 are produced in the reactions

$$eZ \to eZA', \quad (114)$$

$$A' \to \chi_1\chi_2. \quad (115)$$

Here we assume that $m_{\chi_2} > m_{\chi_1}$. In pseudo-Dirac model the decay

$$\chi_2 \to \chi_1 e^+e^- \quad (116)$$

allows to avoid GMB restrictions [74] on the s-wave DM annihilation cross-section. The decay width $\chi_2 \to \chi_1 e^+e^-$ is given by the formula [123]

$$\Gamma(\chi_2 \to \chi_1 e^+e^-) \approx \frac{4\epsilon^2\alpha\alpha_{\rm D}\Delta^5}{15\pi m_{A'}^4}, \quad (117)$$

where $\Delta = m_{\chi_2} - m_{\chi_1}$. For the case of dominant $A' \to e^+e^-$ decay the dark photon decay length is given by the formula [39]

$$l_{A'} = \gamma_{A'}c\tau \approx 0.8\ \text{mm}\times\left(\frac{\gamma_{A'}}{10}\right)\times\left(\frac{10^{-4}}{\epsilon}\right)^2\times\frac{100\ \text{MeV}}{m_{A'}}, \quad (118)$$

where $\gamma_{A'} = \frac{E_{A'}}{m_{A'}}$. The analogous formula for $\chi_2 \to \chi_1 e^+e^-$ decay length is

$$l_{\chi_2} = \gamma_{\chi_2}c\tau \approx 0.8\ \text{mm}\times\left(\frac{\gamma_{\chi_2}}{10}\right)\times\left(\frac{10^{-4}}{\varepsilon}\right)^2\times\kappa^{-1}\times\frac{100\ \text{MeV}}{m_{A'}}. \quad (119)$$

Here $\gamma_{\chi_2} = \frac{E_{\chi_2}}{m_{\chi_2}}$ and $\kappa = \frac{4\alpha_{\rm D}\Delta^5}{5\pi m_A^5}$. As a numerical example we use the point [123] $m_{A'} = 3m_{\chi_1}$, $\Delta = 0.4m_{\chi_1}$ and $\alpha_{\rm D} = 0.1$. For this point we find that

$$l_{\chi_2} = \gamma_{\chi_2}c\tau \approx 0.8\ \text{mm}\times\left(\frac{\gamma_{\chi_2}}{10}\right)\times\left(\frac{10^{-4}}{\epsilon}\right)^2\times\frac{100\ \text{MeV}}{m_{A'}}\times 0.43\times 10^6. \quad (120)$$

For NA64 experiment with 100 GeV electron beam the A' energy is ~ 100 GeV and approximately $E_{\chi_2} \sim \frac{E_{A'}}{2} \approx 50$ GeV. As a crude estimate we shall use $\gamma_{\chi_2} = \frac{50\ \text{GeV}}{m_{\chi_2}}$. As a result we find

$$l_{\chi_2} \equiv \gamma_{\chi_2}c\tau \approx 7.6\ \text{cm}\left(\frac{10^{-1}}{\epsilon}\right)^2\times\left(\frac{100\ \text{MeV}}{m_{A'}}\right)^2. \quad (121)$$

For instance, for $m_{A'} = 100$ MeV and $\epsilon = 10^{-2}$

$$l_{\chi_2} \approx 8\ \text{m}. \quad (122)$$

So the problem arises—is it possible to derive bounds on ε^2 at finite l_{χ_2} from NA64 data? The NA64 experiment for the search for invisible A' decays consists of ECAL with the length 60 cm. Also we have 3 HCAL modules each with $l_{\rm HCAL} = 170$ cm and the distance between the end of the ECAL and the begining of the HCAL modules is 80 cm. So the distance between the begining of ECAL and the end of the last HCAL section(the end of NA64 experiment) is $l_{\rm exp} = 6.5$ m. The active zone of ECAL is

$l_{\mathrm{ECAL,act}} \approx 45$ cm. Suppose the A' is produced in ECAL and immediately decays into $\chi_2\chi_1$ (this assumption is correct since $\alpha_D = 0.1$ and $\Gamma(A' \to \chi_2\chi_1)$ is not small) and χ_2 decays into $\chi_1 e^+e^-$ with the decay length l_{χ_2}. The probability that χ_2 does not decay within NA64, i.e. between the ECAL and the HCAL, is

$$P_{\chi_2}(\text{outside decay}) = \exp\left(-\frac{l_{\mathrm{exp}}}{l_{\chi_2}}\right), \quad (123)$$

where l_{χ_2} is the χ_2 decay length. We can use the NA64 results on the search for invisible dark photon decays. The bound on mixing parameter is

$$\epsilon^2 \le \epsilon^2_{\mathrm{NA64,up}} \times (P_{\chi_2}(\text{outside decay}))^{-1}, \quad (124)$$

where $\epsilon^2_{\mathrm{NA64,up}}$ is the NA64 upper bound [34] obtained in the assumption that $\mathrm{Br}(A' \to \text{invisible}) = 100\%$. Also the situation with χ_2 decaying withing the ECAL is possible. In this case we have missing energy due to decay chain $A' \to \chi_1\chi_2 \to \chi_1\chi_1 e^+e^-$ and nonobservation of 2 χ_1 particles. The average missing energy in this decay is $E_{\mathrm{miss}} \approx 0.5E_{A'} + \frac{1}{3}E_A$, and it is bigger than the used in NA64 missing energy cut $E_{\mathrm{miss}} > E_{\mathrm{miss,cut}} = 50$ GeV. So we can detect the events related with the χ_2 decay within ECAL by the measurement of missing energy. The probability that χ_2 decays within ECAL active zone is

$$P_{\chi_2}(\text{decaysin ECAL}) = 1 - \exp\left(-\frac{l_{\mathrm{ECAL,act}}}{l_{\chi_2}}\right). \quad (125)$$

So total probability of the χ_2 detection with the use of energy missing cut is

$$P_{\chi_2} = P_{\chi_2}(\text{decaysin ECAL}) + P_{\chi_2}(\text{outside decay}) \times \left(1 - \exp\left(-\frac{l_{\mathrm{ECAL,act}}}{l_{\chi_2}}\right)\right) + \exp\left(-\frac{l_{\mathrm{exp}}}{l_{\chi_2}}\right). \quad (126)$$

For arbitrary l_{χ_2} the expression (126) for P_{χ_2} has minimal value at

$$l_{\mathrm{exp}} \exp\left(-\frac{l_{\mathrm{exp}}}{l_{\chi_2,\mathrm{min}}}\right) = l_{\mathrm{ECAL,act}} \exp\left(-\frac{l_{\mathrm{ECAL,act}}}{l_{\chi_2,\mathrm{min}}}\right), \quad (127)$$

or

$$l_{\chi_2,\mathrm{min}} = \frac{l_{\mathrm{exp}} - l_{\mathrm{ECAL,act}}}{\ln\left(\frac{l_{\mathrm{exp}}}{l_{\mathrm{ECAL,act}}}\right)}, \quad (128)$$

and $P_{\chi_2,\mathrm{min}}$ is

$$P_{\chi_2,\mathrm{min}} = \left(1 - \exp\left(-\frac{l_{\mathrm{ECAL,act}}}{l_{\mathrm{exp}} - l_{\mathrm{ECAL,act}}} \ln\frac{l_{\mathrm{exp}}}{l_{\mathrm{ECAL,act}}}\right) + \exp\left(-\frac{l_{\mathrm{exp}}}{l_{\mathrm{exp}} - l_{\mathrm{ECAL,act}}} \ln\frac{l_{\mathrm{exp}}}{l_{\mathrm{ECAL,act}}}\right)\right). \quad (129)$$

Numerically for $l_{\mathrm{exp}} = 650$ cm and $l_{\mathrm{ECAL,exp}} = 40$ cm we find

$$P_{\chi_2,\mathrm{min}} \approx 0.22. \quad (130)$$

The bound on ϵ^2 reads

$$\epsilon^2 \le \epsilon^2_{\mathrm{NA64,up}} \times (P_{\chi_2,\mathrm{min}})^{-1} \approx 4.5 \times \epsilon^2_{\mathrm{NA64,up}}. \quad (131)$$

Here $\epsilon^2_{\mathrm{NA64,up}}$ is the NA64 bound for the case of invisible A' decay. So we see that NA64 is able to obtain upper bound on ϵ^2 parameter for the case of visible A' decay with large missing energy in a model independent way. The knowledge of l_{χ_2} allows to improve the bound (131).

ACKNOWLEDGMENTS

We are indebted to our colleagues from the NA64 Collaborations, in particular to P. Crivelli, D.V. Kirpichnikov, M.M. Kirsanov and V. Lyubovitsky, for many useful discussions and comments. We would also like to thank R. Dusaev for his help in designing and preparing several figures.

REFERENCES

1. E. W. Kolb and M. S. Turner, "The early Universe," Front. Phys. **69**, 1–547 (1990).
2. D. S. Gorbunov and V. A. Rubakov, *Introduction to the Theory of the Early Universe* (World Scientific Publishing Co. Pt. Ltd., 2011).
3. C. Boehm and P. Fayet, "Scalar dark matter candidates," Nucl. Phys. B **683**, 219–263 (2004).
4. J. Alexander et al. (Dark Sector Collab.), *Dark Sectors 2016 Workshop: Community Report* (2016); arXiv: 1608.08632.
5. M. Battaglieri et al., *US Cosmic Visions: New Ideas in Dark Matter 2017: Community Report* (2017); arXiv: 1707.04591.
6. H.-S. Lee, "Muon $g-2$ anomaly and dark leptonic gauge boson," Phys. Rev. D **90**, 091702 (2014).
7. A. Berlin, N. Blinov, G. Krnjaic, P. Schuster, and N. Toro, "Dark matter, millicharges, axion and scalar particles, gauge bosons, and other new physics with LDMX," Phys. Rev. D **99**, 075001 (2019).
8. B. W. Lee and S. Weinberg, "Cosmological lower bound on heavy neutrino masses," Phys. Rev. Lett. **39**, 165–168 (1977).
9. G. Patrignani et al. (Particle Data Group), "Particle data," Chin. Phys. C **40**, 100001 (2016).
10. E. Izaguirre, G. Krnjaic, P. Schuster, and N. Toro, "Testing GeV-scale dark matter with fixed-target miss-

ing momentum experiments," Phys. Rev. D **91**, 094026 (2015).
11. G. Krnjaic, "Probing light thermal dark-matter with a Higgs portal mediator," Phys. Rev. D **94**, 095019 (2016).
12. L. B. Okun, "Limits of electrodynamics: Paraphotons?," Sov. Phys. JETP **56**, 502–510 (1982).
13. B. Holdom, "Two $U(1)$'s and epsilon charge shifts," Phys. Lett. B **166**, 196–198 (1986).
14. G. W. Bennett et al. (Muon g - 2 Collab.), "Final report of the muon E821 anomalous magnetic moment measurement at BNL," Phys. Rev. D **73**, 072003 (2006).
15. M. Davier, A. Hoecker, B. Malaescu, and Z. Zhang, "Reevaluation of the hadronic contributions to the muon $g-2$ and to $\alpha(M_Z)$," Eur. Phys. J. C **71**, 1515–1527 (2011); [Erratum]: Eur. Phys. J. C **72,** 1874 (2012).
16. F. Jegerlehner and R. Szafron, "$\rho^0 - \gamma$ mixing in the neutral channel pion form factor and its role in comparing e^+e^- with τ spectral functions," Eur. Phys. J. C **71**, 1632–1641 (2011).
17. K. Hagiwara, R. Liao, A. D. Martin, D. Nomura, and T. Teubner, "$(g-2)_\mu$ and $\alpha(M_Z)$ reevaluated using new precise data," J. Phys. G **38**, 085003 (2011).
18. T. Aoyama, M. Hayakawa, T. Kinoshita, and M. Nio, "Complete tenth-order QED contribution to the muon g – 2," Phys. Rev. Lett. **109**, 111808 (2012).
19. X.-G. He, G. C. Joshi, H. Lew, and R. Volkas, "New Z-prime phenomenology," Phys. Rev. D **43**, 22–24 (1991).
20. R. Foot, "New physics from electric charge quantization?," Mod. Phys. Lett. A **6**, 527–530 (1991).
21. X.-Ge. He, G. C. Joshi, H. Lew, and R. Volkas, "Simplest Z' model," Phys. Rev. D **44**, 2118–2132 (1991).
22. S. N. Gninenko and N. V. Krasnikov, "The muon anomalous magnetic moment and a new light gauge boson," Phys. Lett. B **513**, 119—123 (2001).
23. S. Baek, N. G. Deshpande, and X. G. He, "Muon anomalous $g-2$ and gauged $L_\mu - L_\tau$ models," Phys. Rev. D **64**, 055006 (2001).
24. E. Ma, D. Roy, and S. Roy, "Gauged $L_\mu - L_\tau$ with large muon anomalous magnetic moment and the bimaximal mixing of neutrinos," Phys. Lett. B **525**, 101–106 (2002).
25. N. V. Krasnikov, *The Muon (g - 2) Anomaly and a New Light Vector Boson* (2017); arXiv:1702.04596.
26. A. Krasznahorskay et al. (Atomki Collab.), "Observation of anomalous internal pair creation in Be8: A possible indication of a light, neutral boson," Phys. Rev. Lett. **116**, 042501 (2016).
27. N. V. Krasnikov, *Light Scalars, $g_\mu - 2$ Muon Anomaly and Dark Matter in a Model with a Higgs Democracy* (2017); arXiv:1707.00508.
28. S. N. Gninenko and N. V. Krasnikov, "Probing the muon $g_\mu - 2$ anomaly, $L\mu - L_\tau$ gauge boson and Dark Matter in dark photon experiments," Phys. Lett. B **783**, 24–30 (2018).
29. C.-Yu. Chen, J. Kozaczuk, and Yi-M. Zhong, "Exploring leptophilic dark matter with NA64 μ," J. High Energy Phys., No. 10, 154–183 (2018).
30. M. Escudero, D. Hopper, G. Krnjaic, and M. Pierre, "Cosmology with a very light $L_\mu - L_\tau$ gauge boson," J. High Energy Phys., No. 03, 071–096 (2019).
31. S. Andreas et al. (NA64 Collab.), *Proposal for an Experiment to Search for Light Dark Matter at the SPS* (2013); arXiv:1312.3309[hep-ph].
32. D. Banerjee et al. (NA64 Collab.), "Search for invisible decays of sub-GeV dark photons in missing-energy events at the CERN SPS," Phys. Rev. Lett. **118**, 011802 (2017).
33. D. Banerjee et al. (NA64 Collab.), "Search for vector mediator of dark matter production in invisible decay mode," Phys. Rev. D **97**, 072002 (2018).
34. D. Banerjee et al. (NA64 Collab.), "Dark matter search in the missing energy events with NA64," Phys. Rev. Lett. **123**, 121801 (2019).
35. D. Banerjee et al. (NA64 Collab.), "Search for a hypothetical 16.7 MeV gauge boson and dark photons in the NA64 Experiment at CERN," Phys. Rev. Lett. **120**, 231802 (2018).
36. H. Davoudiasl and W. I. Marciano, "Running of the $U(1)$ coupling in the dark sector," Phys. Rev. D **92**, 035008 (2015).
37. D. Tucker-Smith and N. Weiner, "Inelastic dark matter," Phys. Rev. D **64**, 043502 (2001).
38. T. Cherghetta, J. Kersten, K. Olive, and M. Pospelov, *The Price of Tiny Kinetic Mixing* (2019); arXiv: 1909.00696.
39. J. D. Bjorken, R. Essig, P. Schuster, and N. Toro, "New fixed-target experiments to search for dark gauge forces," Phys. Rev. D **80**, 075018 (2009).
40. Yu-S. Liu, D. McKeenn, and G. A. Miller, "Validity of the Weizsacker-Williams approximation and the analysis of beam dump experiments: Production of an axion, a dark photon, or a new axial-vector boson," Phys. Rev. D **96**, 01604 (2017).
41. S. N. Gninenko, D. V. Kirpichnikov, M. M. Kirsanov, and N. V. Krasnikov, "The exact tree-level calculation of the dark photon production in high-energy electron scattering at the CERN SPS," Phys. Lett. B **782**, 406–414 (2018).
42. A. E. Dorokhov, A. E. Radzhabov, and A. S. Zhevlakov, "The muon $g-2$: Retrospective and future," EPJ Web Conf. **125**, 02007–02016 (2016).
43. F. Jegelehener and A. Nyffeler, "The muon $g-2$," Phys. Rep. **477**, 1–134 (2009).
44. S. N. Gninenko and N. V. Krasnikov, "The SM extensions with additional light scalar singlet, nonrenormalizable Yukawa interactions and $(g-2)_\mu$," EPJ Web Conf. **125**, 02001 (2017).
45. B. Aubert et al. (BaBar and Belle Collabs.), "The physics of the B factories," Eur. Phys. J. C **74**, 3026–3954 (2014).
46. H. Davoudiasl and W. J. Marciano, "Tale of two anomalies," Phys. Rev. D **98**, 075011 (2018).
47. M. Endo, K. Hamaguchi, and G. Mishima, "Constraints on hidden photon models from electron $g-2$ and hydrogen spectroscopy," Phys. Rev. D **86**, 095029 (2012).
48. S. Abrahamyan et al. (APEX Collab.), "Search for a new gauge boson in electron-nucleus fixed-target scattering by the APEX experiment," Phys. Rev. Lett. **107**, 191804 (2011).

49. H. Merkel et al. (A1 Collab.), "Search at the Mainz microtron for light massive gauge bosons relevant for the muon $g-2$ anomaly," Phys. Rev. Lett. **112**, 2218002 (2014).
50. J. P. Lees et al. (BaBar Collab.), "Search for a Dark Photon in e^+e^- collisions at BaBar," Phys. Rev. Lett. **113**, 201801 (2014).
51. E. Perez del Rio, "Dark forces searches at KLOE-2," Acta Phys. Pol. B **47**, 461–470 (2016).
52. J. R. Batley et al. (NA48/2 Collab.), "Search for the dark photon in π^0 decays," Phys. Lett. B **746**, 178–188.
53. J. P. Lees et al. (BaBar Collab.), "Search for a muonic dark force at BaBar," Phys. Rev. D **94**, 011102 (2016).
54. J. L. Feng, B. Fornal, I. Galon, S. Gardner, J. Smolinsky, T. M. P. Tait, and Ph. Tanedo, "Particle physics models for the 17 MeV anomaly in beryllium nuclear decays," Phys. Rev. D **95**, 035017 (2017).
55. G. Aad et al. (ATLAS Collab.), "Dark-photon searches via Higgs-boson production," J. High Energy Phys., No. 02, **062** (2016).
56. V. Khachatryan et al. (CMS Collab.), "A search for pair production of new light bosons decaying into muons," Phys. Lett. B **752**, 146–168 (2016).
57. R. Aaij et al. (LHCb Collab.), "Search for dark photons produced in 13 TeV collisions," Phys. Rev. Lett. **120**, 061801 (2018).
58. A. V. Artamonov et al. (BNL-E249 Collab.), "New measurement of the $K^+ \to \pi^+\nu\bar{\nu}$ branching ratio," Phys. Rev. D. **79**, 092004 (2009).
59. M. Pospelov, "Secluded $U(1)$ below the weak scale," Phys. Rev. D **80**, 095002 (2009).
60. H. Davoudiasl, H.-S. Lee, and W. J. Marciano, "Muon $(g-2)$, rare kaon decays, and parity violation from dark bosons," Phys. Rev. D **89**, 095006 (2014).
61. R. Essig, K. Mardon, M. Papucci, T. Volansky, and Yi-M. Zhong, "Constraining light dark matter with low-energy e^+e^- colliders," J. High Energy Phys., No. 11, 167–196 (2013).
62. J. P. Lees et al. (BaBar Collab.), "Search for invisible decays of a dark photon produced in e^+e^- collisions at BaBar," Phys. Rev. Lett. **119**, 131804 (2017).
63. J. D. Bjorken et al. (E 137 Collab.), "Search for neutral metastable penetrating particles produced in the SLAC beam dump," Phys. Rev. D **38**, 3375–3420 (1988).
64. A. Bross et al. (E774 Collab.), "A search for shortlived particles produced in an electron beam dump," Phys. Rev. Lett. **67**, 2942–2945 (1991).
65. J. Batell, R. Essig, and Z. Surujon, "Strong constraints on sub-GeV dark sectors from SLAC beam dump E137," Phys. Rev. Lett. **113**, 061801 (2014).
66. S. N. Gninenko, "Stringent limits on the $\pi^0 -> \gamma X; X \to e^+e^-$ decay from neutrino experiments and constraints on new light gauge bosons," Phys. Rev. D **85**, 055027 (2017).
67. S. N. Gninenko, "Constraints on sub-GeV hidden sector gauge bosons from a search for heavy neutrino decays," Phys. Lett. B **713**, 244–248 (2012).
68. L. B. Auerbach et al. (LSND Collab.), "Measurement of electron-neutrino-electron elastic scattering," Phys. Rev. D **63**, 112001 (2001).
69. A. A. Aguilar-Arevalo et al. (MiniBoone Collab.), "Dark matter search in a proton beam dump with MiniBooNE," Phys. Rev. Lett. **118**, 221803 (2017).
70. D. Akimov et al. (COHERENT Collab.), "COHERENT 2018 at the Spallation Neutron Source" (2018); arXiv:1803.09183.
71. D. Akimov et al. (COHERENT Collab.), "Observation of coherent elastic neutrino-nucleus scattering," Science **357**, 1123–1126 (2017).
72. A.-F. Ge and I. M. Shoemaker, "Constraining photon portal dark matter with TEXONO and COHERENT data," J. High Energy Phys., No. 11, 066–079 (2018).
73. W. Almannsofer, S. Gori, M. Pospelov, and I. Yavin, "Neutrino trident production: A powerful probe of new physics with neutrino beams," Phys. Rev. Lett. **113**, 091801 (2014).
74. P. A. R. Ade et al. (Planck Collab.), "Planck 2015 results. XIII. Cosmological parameters," Astron. Astrophys. A **13**, 594–656 (2016).
75. J. Redondo and G. Raffelt, "Solar constraints on hidden photons re-visited," J. Cosmol. Astropart. Phys., No. 08, 034–061 (2013).
76. H. An, M. Pospelov, and J. Pradler, "New stellar constraints on dark photons," Phys. Lett. B **725**, 190–195 (2013).
77. J. N. Chang, R. Essig, and S. M. McDermott, "Supernova 1987A constraints on sub-GeV dark sectors, millicharged particles, the QCD axion, and an axion-like particle," J. High Energy Phys., No. 09, 051–080 (2018).
78. R. V. Wagoner, W. A. Fowler, and F. Hoyle, "On the synthesis of elements at very high temperatures," Astrophys. J. **148**, 3–49 (1967).
79. B. Ahlgren, T. Ohlsson, and S. Zhou, "Comment on 'Is dark matter with long-range interactions a solution to all small-scale problems of cold dark matter cosmology?'," Phys. Rev. Lett. **111**, 199001 (2013).
80. C. Boehm, M. J. Dolan, and C. McCabe, "A lower bound on the mass of cold thermal dark matter from Planck," J. Cosmol. Astropart. Phys., No. 08, 041–053 (2013).
81. A. Fradette, M. Pospelov, J. Pradler, and A. Ritz, "Cosmological constraints on very dark photons," Phys. Rev. D **90**, 035022 (2014).
82. C. Boehm, M. J. Dolan, and C. McCabe, "A lower bound on the mass of cold thermal dark matter from Planck," J. Cosmol. Astropart. Phys., No. 08, 041–053 (2013).
83. Y. S. Jeong, C. S. Kim, and H.-S. Lee, "Constraints on the $U(1)_L$ gauge boson in a wide mass range," Int. J. Mod. Phys. A **31**, 1650059 (2016).
84. R. Essig, J. Mandon, and T. Volansku, "Direct detection of sub-GeV dark matter," Phys. Rev. D **85**, 076007 (2012).
85. E. Aprile et al. (XENON1T Collab.), "Light dark matter search with ionization signals in XENON1T," Phys. Rev. Lett. **122**, 141301 (2019).
86. S. N. Gninenko, "Search for MeV dark matter photons in a light-shining-through-walls experiment at CERN," Phys. Rev. D **89**, 075008 (2014).
87. D. Banerjee, P. Crivelli, and A. Rubbia, "Beam purity for light dark matter search in beam dump experiments," Adv. High Energy Phys. **2015**, 105730 (2015).

88. S. N. Gninenko, N. V. Krasnikov, M. M. Kirsanov, and D. V. Kirpichnikov, "Missing energy signature from invisible decays of dark photons at the CERN SPS," Phys. Rev. D **94**, 095025 (2016).
89. G. S. Atoian, V. A. Gladyshev, S. N. Gninenko, V. V. Isakov, A. V. Kovzelev, E. A. Monich, A. A. Poblaguev, A. L. Proskuryakov, and I. N. Semenyuk, "A lead scintillation electromagnetic calorimeter with wavelength fiber readout," Nucl. Instrum. Methods, Sect. A **320**, 144–154 (1992).
90. S. Agostinelli et al. (GEANT4 Collab.), "Geant4 manual," Nucl. Instrum. Methods, Sect. A **506**, 250–303 (2003).
91. S. N. Gninenko, D. V. Kirpichnikov, M. M. Kirsanov, and N. V. Krasnikov, "Combined search for light dark matter with electron and muon beams at NA64," Phys. Lett. B **796**, 117–122 (2019).
92. J. L. Feng and J. Smolinsky, "Impact of a resonance on thermal targets for invisible dark photon searches," Phys. Rev. D **96**, 095022 (2017).
93. J. Kozaczuk, "Dark photons from nuclear transitions," Phys. Rev D **97**, 015014 (2018).
94. Ch.-W. Chiang and P.-Y. Tseng, "Probing a dark photon using rare leptonic kaon and pion decays," Phys. Lett. B **767**, 289–294 (2017).
95. X. Zhang and G. A. Miller, "Can nuclear physics explain the anomaly observed in the internal pair production in the Beryllium-8 nucleus?," Phys. Lett. B **773**, 159–163 (2017).
96. I. Alikhanov and E. A. Paschos, "Searching for new light gauge boson at e^+e^- colliders," Phys. Rev. D **97**, 115004 (2018).
97. Y. Liang, L.-B. Chen, and C.-F. Qiao, "X(16.7) as the solution of the NuTev anomaly," Chin. Phys. C **41**, 063105–063111 (2017).
98. B. Fornal, "Is there a sign of new physics in Beryllium transitions?," Int. J. Mod. Phys. A **32**, 1730020 (2017).
99. P. Fayet, "The light U boson as the mediator of new force coupled to a combination of Q, B, K and dark matter," Eur. Phys. J. C **77**, 53–66 (2017).
100. D. Banerjee et al. (NA64 Collab.), *Improved Limits on a Hypothetical X(16.7) Boson and a Dark Photon Decaying into e^+e^- Pairs* (2019); arXiv:1912.11389.
101. N. V. Krasnikov, *Implications of Last NA64 Results and the Electron $g_e - 2$ Anomaly for the X(16.7) Boson Survival* (2019); arXiv:1912.11689.
102. A. J. Krasznahorkay et al. (Atomki Collab.), *New Evidence Supporting the Existence of the Hypothetic X17 Particle* (2019); arXiv:1910.10459v1.
103. T. Araki, F. Kaneko, T. Ota, J. Sato, and T. Shimomura, "MeV scale leptonic force for cosmic neutrino and muon anomalous magnetic moment," Phys. Rev. D **93**, 01304 (2016).
104. G. Bellini et al. (Borexino Collab.), "Precision measurement of 7Be solar neutrino interaction rate in Borexino," Phys. Rev. Lett. **107**, 141302 (2011).
105. W. Altmannshofer, S. Gori, M. Pospelov, and I. Yavin, "Neutrino trident production: A powerful probe of new physics with neutrino beams," Phys. Rev. Lett. **113**, 091801 (2014).
106. A. Kamada and H.-B. Yu, "Coherent propagation of PeV neutrinos and the dip in the neutrino spectrum at IceCube," Phys. Rev. D **92**, 113004 (2015).
107. T. Araki, S. Hoshino, T. Ota, J. Sato, and T. Shimomura, "Detecting the $L_\mu - L_\tau$ gauge boson at Belle2," Phys. Rev. D **95**, 055006 (2017).
108. M. Battaglieri et al. (BDX Collab.), *Dark Matter Search in a Beam-Dump eXperiment(BDX)* (2017); arXiv: 1712.0518.
109. A. Celentano, "Dark sector searches at Jefferson laboratory," J. Phys.: Conf. Ser. **770**, 012040 (2016).
110. T. Akesson et al. (LDMX Collab.), *Light Dark Matter Experiment (LDMX)* (2018); arXiv:1808.05219.
111. S. N. Gninenko, N. V. Krasnikov, and V. A. Matveev, "Muon $g - 2$ and searches for a new leptophobic sub-GeV dark boson in a missing-energy experiment at CERN," Phys. Rev. D **91**, 095015 (2015).
112. D. Banerjee et al. (NA64 Collab.), *Proposal for an Experiment to Search for Dark Sector Particles Weakly Coupled to Muon at the SPS* (2019); CERN-SPSC-2019-002/SPSC-P-359.
113. C. Chen, M. Pospelov, and Y. Zhong, "Muon beam dump experiments to probe the dark sector," Phys. Rev. D **95**, 11505 (2017).
114. Y. Kahn, G. Krnjaic, and N. Tran, "M^3: A new muon missing experiment to probe $(g - 2)_\mu$ and dark matter at Fermilab," J. High Energy Phys., No. 09, 153–181 (2018).
115. Chien-Yi. Chen, J. Kozaczuk, and Zhong Yi-Ming, "Exploring leptophilic dark matter with NA64-μ," J. High Energy Phys., No. 10, 154–173 (2018).
116. S. Alekhin et al. (SHiP Collab.), "A facility to search for hidden particles at the CERN SPS: The SHiP physics case," Rep. Progr. Phys. **79**, 124201 (2016).
117. E. Kou et al. (Belle-2 Collab.), *The Belle II Physics Book* (2018); arXiv:1808.10567[hep-ex]; Belle-II collaboration. https://www.belle2.org.
118. L. Doria, P. Achenbach, M. Christmann, A. Denig, P. Gulker, and H. Merkel, *Search for Light Dark Matter with the MESA Accelerator* (2018); arXiv:1809.07168.
119. V. Kozhuharov et al. (PADME Collab.), "PADME: Searching for dark mediator at the Frascati BTF," Nuovo Cimento **40**, 192–208 (2017).
120. B. Wojtsekhowski et al. (VEPP-3 Collab.), "Searching for a dark photon: Project of the experiment at VEPP-3," J. Instrum. **13**, P02021 (2018).
121. J. Balewski et al. (Darklight Collab.), *The DarkLight Experiment: A Precision Search for New Physics at Low Energies* (2014); arXiv:1412.4717.
122. P. Gondolo and G. Gelmini, "Cosmic abundances of stable particles; improved analysis," Nucl. Phys. B **360**, 145–187 (1991).
123. G. Mohlabeng, "Revisiting the dark photon explanation of the muon anomalous magnetic moment," Phys. Rev. D **99**, 115001 (2019).